Forcing of oceanic mean flows by dissipating internal tides

Nicolas Grisouard† and Oliver Bühler

Courant Institute of Mathematical Sciences, New York University, 251 Mercer Street,
New York, NY 10012-1185, USA

We present a theoretical and numerical study of the effective mean force exerted on an oceanic mean flow due to the presence of small-amplitude internal waves that are forced by the oscillatory flow of a barotropic tide over undulating topography and are also subject to dissipation. This extends the classic lee-wave drag problem of atmospheric wave–mean interaction theory to a more complicated oceanographic setting, because now the steady lee waves are replaced by oscillatory internal tides and, most importantly, because now the three-dimensional oceanic mean flow is defined by time averaging over the fast tidal cycles rather than by the zonal averaging familiar from atmospheric theory. Although the details of our computation are quite different, we recover the main action-at-a-distance result from the atmospheric setting, namely that the effective mean force that is felt by the mean flow is located in regions of wave dissipation, and not necessarily near the topographic wave source. Specifically, we derive an explicit expression for the effective mean force at leading order using a perturbation series in small wave amplitude within the framework of generalized Lagrangian-mean theory, discuss in detail the range of situations in which a strong, secularly growing mean-flow response can be expected, and then compute the effective mean force numerically in a number of idealized examples with simple topographies.

1. Introduction

Internal gravity waves play an essential part in the global-scale dynamics of both the atmosphere and the oceans. This is despite their comparatively short spatial and temporal scales, which for the most part renders them unresolvable in present-day computer models for the global circulation. In the atmosphere, the most important internal-wave effect is the wave-induced vertical transport of angular momentum and the concomitant effective force exerted on the flow in locations where the waves break or otherwise dissipate. Here the simplest relevant thought experiment is the lee-wave problem, i.e. a steady wind blowing over undulating topography that generates upward propagating internal waves with zero absolute frequency. There is a net drag force on the topography and, in the simplest setting of zonal averaging applied to a horizontally homogeneous mean flow, there is an equal-and-opposite effective force exerted on the mean flow in the regions of wave dissipation. Remarkably, these lee waves are felt

† Email address for correspondence: grisouard@cims.nyu.edu

by the mean flow not where the waves are generated but only where the waves are dissipated.

The theoretical underpinnings for the computation of the effective force exerted by dissipating internal waves in the atmosphere are by now very well established (e.g. Bühler 2009, § 6), and form the basis for all parametrization schemes of such effects in numerical models. Basically, this classic theory works by exploiting the zonal symmetry of the assumed wind profile, which makes zonal averaging a natural procedure in order to distinguish the mean and disturbance parts of the flow. Clearly, a direct application of this classic theory to the ocean immediately runs into problems because most oceanic currents are not zonally symmetric even to a first approximation and therefore one cannot simply apply the classic theory, which has been built around this approximation. (There is one notable exception, namely the antarctic circumpolar current, which encircles the globe in a manner similar to atmospheric currents.)

Little progress has been made on this problem, partly for the aforementioned technical reasons, but mostly because oceanographic interest in internal waves is focused on their contribution to small-scale mixing and not on momentum transfers. Indeed, in recent years there has been significant progress in understanding the role of internal waves in the mixing processes in the deep ocean. This follows the observational discovery some fifteen years ago that small-scale turbulence levels are greatly elevated above regions of strong topography, a finding that has been linked to increased internal wave activity in these regions (e.g. Polzin *et al.* 1997; Ledwell *et al.* 2000). Basically, the intermittent breaking of internal waves produces patches of three-dimensional turbulence, and the small-scale turbulent mixing across these patches then contributes to the transport of fluid particles across the stable-stratification surfaces of the ocean, which is a significant part of the functioning of the global overturning circulation of the ocean. Several source mechanisms for such topographic internal waves exist. For example, recently Nikurashin & Ferrari (2010*a*,*b*) have investigated two-dimensional lee waves produced by geostrophic currents over periodic random ocean topography, which is similar to the atmospheric lee-wave problem and can to some extent be studied using zonal averaging.

Probably the strongest source mechanism for topographic internal waves in the ocean is provided by the barotropic tides, i.e. the relentless back-and-forth sloshing of the entire oceanic water column in response to lunar and solar gravitational forcing. This leads to the generation of so-called internal tides, which are topographically generated internal waves with frequencies dominated by tidal frequencies. There have been numerous internal-tide studies in recent years (for a review see Garrett & Kunze 2007), which mostly focus on the wave energy budget and its heuristic links to wave-induced turbulent mixing (e.g. Muller & Bühler 2009).

In the present paper we augment these earlier internal-tide studies that were focused on wave-induced mixing by computing the effective force exerted on the mean flow due to wave dissipation. Basically, our aim is to use the well-studied example of internal tides in order to put on record a detailed wave–mean interaction problem involving internal waves and three-dimensional mean flows in the ocean. In keeping with oceanographic requirements, here we define the mean flow not with zonal averaging, but with a time average over the fast tidal oscillations. In other words, we retain the mean flow as a fully three-dimensional time-dependent flow, but we average over the fast time scale of the internal tides and replace the action of the waves on the mean flow by a suitably defined effective mean force. This makes the oceanic theory slightly more difficult than its atmospheric counterpart.

The theory is worked out in a typical scenario for internal-tide studies: a finite-depth ocean modelled as a Boussinesq fluid where internal tides are first generated by tidal sloshing over localized topography and then propagate away to horizontal infinity. Just as in the atmospheric case, we will recover that the mean flow is affected by the stationary waves in regions of significant wave dissipation, but not necessarily near the topographic source region.

In order to facilitate our study we use the simplest model for internal tides, which combines small-amplitude topography with a small-excursion assumption for the barotropic tide, i.e. the ratio between tidally induced horizontal particle excursions and the scale of the localized topography is assumed to be small. By using uniform rotation and stratification and no basic flow we also ignore all effects to do with shear, background turbulence, or other forms of inhomogeneity in the water column. We also use a crude and simplistic model for wave dissipation by allowing for linear damping in the buoyancy equation. This is blatantly unrealistic for the ocean, but allows a simple handle with which to model the wave–mean interactions due to wave breaking in a qualitatively correct way. In this set-up the sought effective mean force arises at second order in wave amplitude, so we have a standard problem in small-amplitude wave–mean interaction theory to solve, i.e. the fluid flow is studied by a regular perturbation approach based on ascending orders in wave amplitude. We find it convenient to use the generalized Lagrangian-mean formalism to compute the leading-order mean-flow response, because in the present setting the formalism offers the simplest mean-flow boundary conditions as well as a useful handle on the evolution equation for the Lagrangian-mean potential vorticity (PV), central to an efficient description of the three-dimensional mean-flow dynamics.

We solve for the linear waves using a Green's function approach similar to that of Llewellyn Smith & Young (2002), but slightly extended to yield smooth results over the topography. Our main theoretical result is the expression for the nonlinear effective mean force and its curl in (4.10) and (4.11) below. The curl of this force encapsulates the entire forcing of the second-order mean flow due to the first-order waves, and the vertical component of its curl captures the all-important forcing of the Lagrangian-mean PV. This is the most important part of the wave–mean interactions in this problem, because secular growth of the mean-flow response is inevitably linked to secular growth of the PV, so the strongest interactions are those that project onto the PV dynamics. We then illustrate the effective force structure with a number of idealized examples with different topography shapes for which we compute the full solution numerically. Also, there is a superficial resemblance between our results and those of a few other studies, most notably tidal rectification studies, so we briefly discuss the relationship between these theories.

The layout of the paper is as follows. The governing equations and the flow domain are described in §2 and the linear wave solution is derived in §3. The Lagrangian-mean equations for the second-order mean-flow response and the effective mean force are derived in §4. The conditions for secularly growing mean-flow responses in various configurations are discussed in §5 and numerical examples for different topography shapes are presented in §6. Concluding comments are offered in §7.

2. Physical and mathematical model for dissipating internal waves

2.1. *Model ocean and barotropic tidal flow*

The basic ocean set-up is illustrated in figure 1. We consider a standard three-dimensional Boussinesq fluid model in a domain that is unbounded in the horizontal
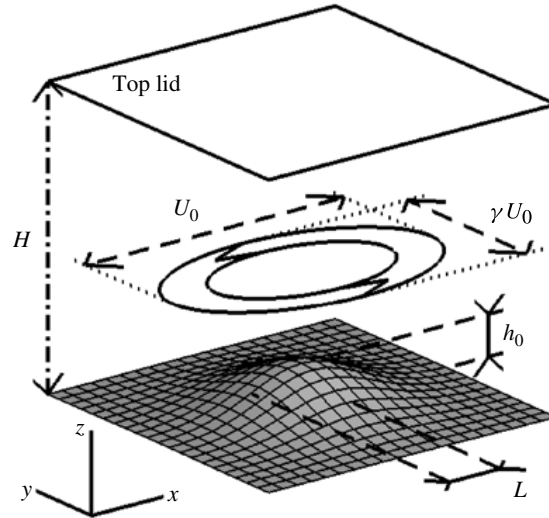
FIGURE 1. Three-dimensional set-up: a rotary barotropic tide of velocity amplitude U_0 along its major axis and γU_0 along its minor axis flows over a topography of height h_0 and typical slope h_0/L. The buoyancy frequency N and the Coriolis frequency f, both constant, are not represented. Note that the width of the barotropic tidal ellipse does not scale with the width of the topography.

directions but finite in the vertical. A Cartesian system of coordinates (x, y, z) is used such that a rigid flat lid modelling the ocean surface is located at $z = H$ whilst an undulating lower boundary described by bottom topography is located at $z = h(x, y)$. We assume that the topography is compact, i.e. h is essentially zero outside some finite region, which makes undisturbed wave propagation to horizontal infinity a well-defined concept. The fluid is rotating and although it is unbounded in the horizontal, it is assumed to be of small enough extent for the Coriolis frequency $f > 0$ to be taken as constant; in other words, we are using the standard f-plane approximation. The density is decreasing with height with constant, real buoyancy frequency N and hence can support internal gravity waves. N and the latitude are chosen to be large enough for the non-traditional Coriolis terms to be neglected.

In the absence of topography we envisage that oscillatory tidal forces set the entire ocean into an oscillation with some frequency $\omega > f$ such that there is a barotropic tide with velocity

$$\boldsymbol{U} = U_0(\cos \omega t, \gamma \sin \omega t, 0). \tag{2.1}$$

Here the adjustable parameter $\gamma \in [-1, +1]$ measures the ellipticity of the barotropic tide (if $\gamma \neq 0$, the tide is described as rotary). For example, $\gamma = -f/\omega$ in a simple model problem in which the tidal forces act in the x-direction only. In the presence of small-amplitude topography with typical height h_0 and horizontal scale L, say, the barotropic tide will interact with the topography and create so-called internal tides, which can radiate away from the topography (Bell 1975). It is the mean flow forced by the dissipation of these internal tides that is our main interest. We will fix the numerical values of some of the parameters throughout this study: $H = 4$ km is a typical value away from continental shelves, $f = 10^{-4}$ s^{-1} is correct at latitude 45°N, $N = 10^{-3}$ s^{-1} is a typical value for the abyssal ocean and $\omega = 1.4 \times 10^{-4}$ s^{-1} is a good approximation of the frequency of the semi-diurnal tide. Note that $f < \omega < N$, so

we are considering propagating internal waves. For the topography we set $h_0 = 100$ m and $L = 10$ km. We also choose $U_0 = 1.4$ cm s^{-1}, a rather low yet realistic value for the bottom of the ocean.

2.2. *Two asymptotic approximations for the topography*

There are two non-dimensional parameters related to the height h_0 and the width L of the topography, and we will build up our model based on the fact that given the dimensional parameters listed previously, both of these are small. They are

$$\epsilon = \frac{U_0}{\omega L} \ll 1 \quad \text{and} \quad a = \frac{h_0}{\mu L} \ll 1, \tag{2.2}$$

where $\mu = \sqrt{(\omega^2 - f^2)/(N^2 - \omega^2)}$ is the natural slope of internal waves with intrinsic frequency ω. Here the excursion parameter ϵ compares the tide-induced horizontal particle displacements of size U_0/ω against the typical horizontal scale of the topography L. As was first noticed by Zeilon (1912) for the two-layer case and Bell (1975) for the continuously stratified case, the temporal frequency spectrum of the internal wave field generated by the tide–topography interaction contains an infinite number of harmonics of ω unless $\epsilon \ll 1$. To make this assumption requires ensuring that L is large enough, at least a few kilometres; with our choice of parameters

$$\epsilon = \tfrac{1}{100}. \tag{2.3}$$

The amplitude parameter a compares the topography slope h_0/L against μ. For our choice of parameters,

$$\mu \simeq \tfrac{1}{10} \quad \text{and therefore} \quad a \simeq \tfrac{1}{10}. \tag{2.4}$$

The weak topography approximation (WTA) $a \ll 1$, first developed by Bell (1975) as well, has two important simplifying consequences. First, it allows one to apply the lower boundary condition at a flat bottom $z = 0$ rather than at the undulating bottom $z = h$. Second, it makes the waves essentially linear and solutions of our problem can be viewed as asymptotic expansions in powers of a, where the basic barotropic flow is $O(1)$, the linear wave field is $O(a)$, and the leading-order mean-flow response arises from nonlinear wave–wave interactions and is therefore $O(a^2)$. Now, we will perform this expansion in powers of a but we will not attempt to expand in powers of the other small parameter, ϵ. Strictly speaking, this requires the restriction $\epsilon \ll a$ in order for it to make sense to compute higher-order terms in a but not in ϵ. In our set-up $\epsilon/a \simeq 1/10$, so there is scope for this scaling regime, although we have not attempted to justify it rigorously.

2.3. *Governing equations in a co-moving frame*

In the original frame of reference with coordinates (x, y, z) the topography is at rest and the standard Boussinesq equations hold (after addition of suitable gravitational forcing terms for the barotropic tide). However, the total fluid velocity is $\boldsymbol{U} + \boldsymbol{u}$ in that frame, where $\boldsymbol{u}$ is the velocity in excess of the barotropic tide, and advection terms involving the tidal velocity $\boldsymbol{U}$ then appear in the governing equations. These advection terms can be eliminated from the differential equations by switching to a co-moving reference frame attached to the motion of the barotropic tide. In this frame the ocean is at rest but now the topography is moving, which incidentally is often the way in which laboratory experiments on internal tides are actually conducted.

We therefore switch to co-moving Cartesian coordinates defined by

$$(x, y, z) = (x - X(t), y - Y(t), z) = \left(x - \frac{U_0}{\omega} \sin \omega t, \; y + \frac{\gamma U_0}{\omega} \cos \omega t, \; z \right). \quad (2.5)$$

Here the horizontal tidal excursions $X(t)$ and $Y(t)$ are defined by time-integrating (2.1). In this co-moving frame the fluid velocity is given by $\boldsymbol{u}$ only and therefore the fully nonlinear governing equations are

$$\boldsymbol{u}_{,t} + (\boldsymbol{u} \cdot \nabla)\boldsymbol{u} + f\hat{z} \times \boldsymbol{u} = b\hat{z} - \nabla p, \quad (2.6a)$$

$$b_{,t} + (\boldsymbol{u} \cdot \nabla)b + N^2 w = -\alpha b, \quad (2.6b)$$

$$\nabla \cdot \boldsymbol{u} = 0, \quad (2.6c)$$

where subscripts preceded by commas denote partial derivatives, and $\boldsymbol{u} = (u, v, w)$ b and p are the velocity, buoyancy and scaled pressure fields, respectively. Buoyancy is defined as $b = -g\rho'/\rho_0$, where g is acceleration due to gravity, ρ' the density perturbation, ρ_0 a constant reference density, and $\hat{z}$ is the unit vector for the vertical axis.

We have added a linear damping term with constant $\alpha > 0$ to the buoyancy equation as a crude handle on modelling wave dissipation. Other dissipation terms such as viscous stresses would work equally well for our purposes, but would involve more derivatives. Of course, both buoyancy damping and viscous stresses are very crude models for the actual dissipation of oceanic internal waves, which is likely to be dominated by nonlinear wave breaking and three-dimensional turbulence. However, as argued for instance in McIntyre & Norton (1990), the impact on the nonlinear potential vorticity dynamics of real turbulent wave breaking can be mimicked by simpler forms of laminar wave dissipation, provided that the laminar dissipation respects the conservation laws of mass and momentum (Bühler 2000, 2009). For example, as argued in the last two references, we would get the wrong answer for the nonlinear potential vorticity dynamics if we applied Rayleigh damping to the velocity fields in (2.6a). (Note that conserving mechanical energy is a lesser concern in our case: unlike mass and momentum, mechanical energy is not a macroscopically conserved quantity because it can be dissipated into microscopic (e.g. thermal) energy, which is not captured by the Boussinesq equations.)

So, whilst certainly imperfect and simplistic, for the purpose of wave–mean interaction theory the addition of the buoyancy damping term allows us to capture the most salient qualitative aspects of real wave dissipation.

The equations are completed by specifying boundary conditions. In the horizontal directions we apply outward radiation and decay conditions as needed. The no-normal-flow boundary condition at the ocean surface obviously implies

$$w = 0 \quad \text{at } z = H, \quad (2.7)$$

but the lower boundary condition requires a little care. In the co-moving frame the lower boundary is now time dependent and located at $z = h(x + X(t), y + Y(t))$ and therefore the generic no-normal-flow boundary condition $w = \mathrm{D}h/\mathrm{D}t$ takes the form

$$w = (\boldsymbol{u} + \boldsymbol{U}(t)) \cdot \nabla_H h(x + X(t), y + Y(t)) \quad \text{at } z = h(x + X(t), y + Y(t)), \quad (2.8)$$

where ∇_H is the horizontal gradient and where we used $(\dot{X}, \dot{Y}, 0) = \boldsymbol{U}$. Obviously, this complicated nonlinear boundary condition simplifies greatly once we use the asymptotic assumptions of small excursion and small topography amplitude in (2.2). In particular, the small-excursion limit means that we will ignore the tidal

displacements $(X, Y, 0)$ completely in (2.8), which hence reduces to the simpler expression

$$w = (\boldsymbol{u} + \boldsymbol{U}(t)) \cdot \nabla_H h(x, y) \quad \text{at } z = h(x, y). \tag{2.9}$$

Notably, the barotropic tide $\boldsymbol{U}(t)$ enters solely in this lower boundary condition.

3. Linear wave field

As mentioned in §2.2, we now assume that the flow fields can be expanded asymptotically in powers of a:

$$\varphi = \varphi^{(0)} + \varphi^{(1)} + \varphi^{(2)} + O(a^3), \tag{3.1}$$

where φ stands for any flow variable and where $\varphi^{(n)} = O(a^n)$. In this expansion scheme the barotropic tide $\boldsymbol{U}$ has only an $O(1)$ part and the topography h has only an $O(a)$ part, so we omit the superscripts for these fields; the expansions of $(\boldsymbol{u}, p, b)$ all start at $O(a)$. In the next two sections, we look for solutions of our governing equations at each of these orders. Let us solve our problem at $O(a)$ to retrieve the stationary (i.e. steadily oscillating) linear wave field.

3.1. *Linear wave equation*

At $O(a)$, (2.6)–(2.9) become

$$\boldsymbol{u}^{(1)}_{,t} + f\hat{\boldsymbol{z}} \times \boldsymbol{u}^{(1)} = b^{(1)}\hat{\boldsymbol{z}} - \nabla p^{(1)}, \tag{3.2a}$$

$$b^{(1)}_{,t} + N^2 w^{(1)} = -\alpha b^{(1)}, \tag{3.2b}$$

$$\nabla \cdot \boldsymbol{u}^{(1)} = 0, \tag{3.2c}$$

$$w^{(1)}\big|_{z=H} = 0, \quad w^{(1)}\big|_{z=0} = w_0 = \boldsymbol{U}(t) \cdot \nabla_H h. \tag{3.2d}$$

The wave field is monochromatic in time, which allows us to write

$$\varphi^{(1)}(\boldsymbol{r}, z, t) = \frac{\tilde{\varphi}(\boldsymbol{r}, z)e^{-i\omega t} + \tilde{\varphi}^*(\boldsymbol{r}, z)e^{i\omega t}}{2} = \text{Re}\left(\tilde{\varphi}(\boldsymbol{r}, z)e^{-i\omega t}\right), \tag{3.3}$$

where $(\ )^*$ denotes the complex conjugate, $\boldsymbol{r} = (x, y)$ is the horizontal position vector, and Re means taking the real part. Equations (3.2b) and (3.3) then yield

$$\tilde{b} = \frac{N^2}{i\omega - \alpha}\tilde{w}. \tag{3.4}$$

Taking into account the last equation as well as (3.2c) and $[(\nabla \times (3.2a)) \cdot \hat{\boldsymbol{z}}]$, equation $[(\nabla \times (\nabla \times (3.2a))) \cdot \hat{\boldsymbol{z}}]$ gives the equation for the complex-valued vertical velocity:

$$\nabla_H^2 \tilde{w} - (\mu\beta)^2 \tilde{w}_{zz} = 0, \tag{3.5}$$

where ∇_H^2 is the horizontal Laplacian and

$$\beta^2 = \frac{(N^2 - \omega^2)(1 + i\alpha/\omega)}{N^2 - \omega^2 - i\alpha\omega}. \tag{3.6}$$

If $\alpha = 0$, then $\beta = 1$ and one recognizes the usual inviscid hyperbolic internal-wave equation, whose characteristics have a slope μ aligned with the usual group-velocity direction of propagation of the fixed-frequency waves (however, we do not make the assumption of a slowly varying wavetrain here). Equation (3.5) is to be solved using

a radiation condition in the horizontal directions as well as the following vertical boundary conditions:

$$\tilde{w}|_{z=H} = 0; \quad \tilde{w}|_{z=0} = \tilde{w}_0 = \tilde{\boldsymbol{U}} \cdot \boldsymbol{\nabla}_H h, \tag{3.7}$$

where $\tilde{\boldsymbol{U}} = U_0(1, i\gamma)$. We note in passing that applying the hydrostatic approximation, which is common in studies of the present type, only results in simplifying the expressions of μ^2 and β^2 into $(\omega^2 - f^2)/N^2$ and $1 + i\alpha/\omega$, respectively, and does not simplify our problem any further. Hence we will not make this approximation.

3.2. *Derivation of the linear vertical velocity*

We are looking for a solution of (3.5) with the proper radiation and boundary conditions, which we obtain using a Green's function approach. The Green's function we are looking for satisfies (3.5) in the interior of the domain and vanishes at the top and bottom of the domain, except for a point source located at $(\boldsymbol{r}, z) = (\boldsymbol{r}_0, 0)$. Hence, we are looking for a function $G(\boldsymbol{r}, z; \boldsymbol{r}_0)$ such that

$$\nabla_H^2 G - (\mu\beta)^2 G_{,zz} = 0, \tag{3.8a}$$

$$G|_{z=H} = 0, \quad G|_{z=0} = \delta(\boldsymbol{r} - \boldsymbol{r}_0), \tag{3.8b}$$

where δ is Dirac's delta function. The expression for the vertical velocity in the whole domain is then found by integrating $G(\boldsymbol{r}, z; \boldsymbol{r}_0)$ against $\tilde{w}_0(\boldsymbol{r}_0)$ in the horizontal plane.

Solving internal-wave radiation problems using the Green's function approach of Robinson (1969) has been common practice in the literature (e.g. Llewellyn Smith & Young 2003; Pétrélis, Llewellyn Smith & Young 2006; Echeverri & Peacock 2010). However, typically this approach deals with a point source located in the interior of the domain, allowing the Green's function to be written as an infinite sum of sine functions in z that are all zero at the top and bottom of the domain. Obviously, any $\tilde{w}$ thus constructed would not satisfy the lower boundary condition in (3.7) pointwise. To our knowledge, only Llewellyn Smith & Young (2002) solve a radiation problem combining the WTA and a Green's function approach, with the minor difference that they use the hydrostatic approximation. However, they still project their solutions on an infinite set of sine functions that are zero at the bottom boundary, which results in the same problem: the vertical velocities arise from non-zero values at the bottom boundary, but they are zero there by construction of the Green's function. In other words, above non-zero topography the solution based on the infinite sine series in the vertical converges to the true solution only weakly, i.e. in a quadratic integral norm sense. This is perfectly fine for the application that these authors pursued, namely the computation of the outward wave energy flux from an isolated topography feature, because that flux can be computed from the solution evaluated far away from the topography, where the series expansion captures the correct boundary conditions of vanishing vertical velocity.

In contrast, in our case we wish to model the wave field everywhere, including near the topography where the non-uniform convergence of the sine series leads to undesirable Gibbs fringes and very noisy derivatives. We therefore seek a Green's function that is able to pick up the bottom boundary in (3.8b) exactly. One way to do this is to postulate

$$G(\boldsymbol{r}, z; \boldsymbol{r}_0) = \mathscr{G}(\boldsymbol{r}, z; \boldsymbol{r}_0) + \left(1 - \frac{z}{H}\right) \delta(\boldsymbol{r} - \boldsymbol{r}_0), \tag{3.9}$$

where the second term on the right-hand side picks up the lower boundary condition and the remainder $\mathscr{G}$ is now zero at the top and bottom of the domain. Next,

we define

$$\mathscr{G}(\boldsymbol{r}, z; \boldsymbol{r}_0) = \sum_{m=1}^{\infty} \mathscr{G}_m(\boldsymbol{r}; \boldsymbol{r}_0) \sin(k_m z); \quad \mathscr{G}_m(\boldsymbol{r}; \boldsymbol{r}_0) = \frac{2}{H} \int_0^H \mathscr{G}(\boldsymbol{r}, z; \boldsymbol{r}_0) \sin(k_m z) \, \mathrm{d}z, \quad (3.10)$$

where $k_m = m\pi/H$ ($m = 1, 2, \ldots$), multiply (3.8a) by $(2/H) \sin(k_m z)$ and integrate it vertically over $[0, H]$, which requires integrating the $\mathscr{G}_{,zz} \sin(k_m z)$ term by parts twice. The result is the following equation:

$$\nabla_H^2 \mathscr{G}_m(\boldsymbol{r}; \boldsymbol{r}_0) + (\mu\beta k_m)^2 \mathscr{G}_m(\boldsymbol{r}; \boldsymbol{r}_0) = -\frac{2}{\pi m} \nabla_H^2 \delta(\boldsymbol{r} - \boldsymbol{r}_0). \quad (3.11)$$

This is an inhomogeneous two-dimensional Helmholtz equation with wavenumber $\mu\beta k_m$ whose Green's function $g_m(\boldsymbol{r}; \boldsymbol{r}_1)$ is the solution of

$$\nabla_H^2 g_m(\boldsymbol{r}; \boldsymbol{r}_1) + (\mu\beta k_m)^2 g_m(\boldsymbol{r}; \boldsymbol{r}_1) = \delta(\boldsymbol{r} - \boldsymbol{r}_1). \quad (3.12)$$

More specifically, the Green's function which satisfies our radiation condition is (e.g. Barton 1989, § 13)

$$g_m(\boldsymbol{r}; \boldsymbol{r}_1) = \frac{1}{4\mathrm{i}} H_0^{(1)}(\mu\beta k_m |\boldsymbol{r} - \boldsymbol{r}_1|), \quad (3.13)$$

where $H_0^{(1)}$ is the order-zero Hankel function of the first kind and the choice of the root of β^2 is dictated by the fact that waves decay due to dissipation away from the source, i.e. that $\mathrm{Im}(\beta) > 0$, where Im denotes the imaginary part. $\mathscr{G}_m$ is then the result of the integration of g_m against the right-hand side of (3.11):

$$\mathscr{G}_m(\boldsymbol{r}; \boldsymbol{r}_0) = -\frac{2}{\pi m} g_m(\boldsymbol{r}; \boldsymbol{r}_1) \nabla_H^2 \delta(\boldsymbol{r}_1 - \boldsymbol{r}_0) \, \mathrm{d}^2 \boldsymbol{r}_1, \quad (3.14)$$

where ∇_H^2 acts on $\boldsymbol{r}_1$. By definition of the derivative of the Dirac delta function:

$$\begin{aligned} \mathscr{G}_m(\boldsymbol{r}; \boldsymbol{r}_0) &= -\frac{2}{\pi m} \iint_{\mathbb{R}^2} \delta(\boldsymbol{r}_1 - \boldsymbol{r}_0) \nabla_H^2 g_m(\boldsymbol{r}; \boldsymbol{r}_1) \, \mathrm{d}^2 \boldsymbol{r}_1 \\ &= -\frac{2}{\pi m} \nabla_H^2 g_m(\boldsymbol{r}; \boldsymbol{r}_0), \end{aligned} \quad (3.15)$$

where $\mathbb{R}$ represents the set of all real numbers.

Note that ∇_H^2 is supposed to act on $\boldsymbol{r}_0$. However, because g_m is symmetric, we actually invert the roles of $\boldsymbol{r}$ and $\boldsymbol{r}_0$ and consider that ∇_H^2 acts on $\boldsymbol{r}$. Using (3.12) and (3.13), the final expression for G is

$$\begin{aligned} G(\boldsymbol{r}, z; \boldsymbol{r}_0) &= \frac{(\mu\beta)^2}{2\mathrm{i}H} \sum_{m=1}^{\infty} k_m H_0^{(1)}(\mu\beta k_m |\boldsymbol{r} - \boldsymbol{r}_0|) \sin(k_m z) \\ &\quad + \left(1 - \frac{z}{H} - \frac{2}{\pi} \sum_{m=1}^{\infty} \frac{\sin(k_m z)}{m} \right) \delta(\boldsymbol{r} - \boldsymbol{r}_0). \end{aligned} \quad (3.16)$$

The vertical velocity is therefore given by

$$\tilde{w}(\boldsymbol{r}, z) = \frac{(\mu\beta)^2}{2\mathrm{i}H} \sum_{m=1}^{\infty} \mathscr{C}_m(\boldsymbol{r}) \sin(k_m z) + \left(1 - \frac{z}{H} - \frac{2}{\pi} \sum_{m=1}^{\infty} \frac{\sin(k_m z)}{m} \right) \tilde{w}_0(\boldsymbol{r}), \quad (3.17)$$

where

$$\mathscr{C}_m(\boldsymbol{r}) = \iint_{\mathbb{R}^2} k_m H_0^{(1)}(\mu\beta k_m |\boldsymbol{r} - \boldsymbol{r}_0|)\tilde{w}_0(\boldsymbol{r}_0)\,\mathrm{d}^2\boldsymbol{r}_0. \tag{3.18}$$

The first half of (3.17) is analogous to the Green's function solution in Llewellyn Smith & Young (2002) and the second half augments that solution over non-zero topography.

For completeness, we also give the expression for $\tilde{w}$ in the two-dimensional case where $\partial/\partial y = 0$, for which a detailed derivation is provided in appendix A:

$$\tilde{w}(x, z) = \frac{\mu\beta}{\mathrm{i}H} \sum_{m=1}^{\infty} \mathscr{C}_m(x) \sin(k_m z) + \left(1 - \frac{z}{H} - \frac{2}{\pi} \sum_{m=1}^{\infty} \frac{\sin(k_m z)}{m}\right) \tilde{w}_0(x), \tag{3.19}$$

where

$$\mathscr{C}_m(x) = \int_{-\infty}^{\infty} \exp(\mathrm{i}\mu\beta k_m |x - x_0|)\,\tilde{w}_0(x_0)\,\mathrm{d}x_0. \tag{3.20}$$

4. Mean-flow response

4.1. *Strong interactions and potential vorticity*

We now proceed to compute the leading-order mean-flow response to the waves, which arises at $O(a^2)$ in wave amplitude. Here the Eulerian averaging operation that defines the mean flow is a standard multiscale time average, i.e. an average over a time scale that is long compared to the oscillation period of the waves but short compared to the evolution time scale for the mean flow. Equivalently, this amounts to an average over the phase of the monochromatic linear waves. This is a standard problem in wave–mean interaction theory (e.g. Bühler 2009, §8), albeit not a trivial one because of the three-dimensional nature of the mean flow. A key point is to focus on strong wave–mean interactions, i.e. interactions that can force a mean-flow response growing secularly as $O(a^2 t)$ in time. Arguably, weak interactions, which only lead to $O(a^2)$ adjustments of the mean flow that are uniformly bounded in time, can be ignored in the presence of strong interactions, and this simplifies the analysis significantly.

Specifically, in a regular perturbation expansion of the nonlinear fluids equations in wave amplitude, the same linear operator appears at each order in the expansion but with forcing terms on the right-hand side that stem from products of lower-order terms. Clearly, a search for strong interactions then becomes a search for resonantly forced modes of this linear operator. Because the phase-averaged wave field is steady, only the forcing of the zero-frequency mode of the linear Boussinesq operator is captured, which is the usual balanced or vortical mode that can be described by the distribution of potential vorticity throughout the domain. By averaging over a fast time scale, we do not capture any forcing, even resonant, of the mean-flow response related to the gravity-wave modes of the linear operator, whose frequencies are all bounded from below by the Coriolis frequency.

Thus, for a stationary wave field, we expect the mean-flow response to be dominated by the balanced mode, an expectation we now try to confirm by investigating how the wave modes described at $O(a)$ generate the forcing at $O(a^2)$ and how the latter can project on the PV-controlled balanced mode.

4.2. *Generalized Lagrangian-mean equations*

Interactions between waves and mean flows can been studied from both Eulerian and Lagrangian points of view. Although the former usually involves a simpler formalism, Eulerian-mean equations lack an equivalent of the Kelvin circulation theorem (KCT) (e.g. Bühler 2010), which makes it very hard to work with an Eulerian-mean potential vorticity (PV). We, rather, choose to use the generalized Lagrangian-mean (GLM) theory, first developed by Andrews & McIntyre (1978). This theory combines Eulerian features, for instance evaluating all quantities on an Eulerian set of coordinates, and Lagrangian features, such as following the wave-induced displacements of the material particles. This theory makes it relatively easy to define an averaged form of the KCT (e.g. Bühler 2009, §§ 10.2.7 and 10.4.1) and hence a Lagrangian-mean form for the PV.

We note in passing that in the end, the computed $O(a^2)$ fields are Lagrangian and not Eulerian. However, the two are linked by Stokes corrections, which are wave properties which at leading order can be computed from the $O(a)$ solution. As explained by Bühler (2009, § 10.1.1), would be quite easy in our perturbation expansion to subtract the leading-order Stokes correction from the Lagrangian solution to get the mean Eulerian solution, were we looking for it.

Writing down the GLM equations requires first to define some notation. This is the sole purpose of (4.1)–(4.4), which by are no means intended to explain the underlying theory, fully described in other publications (e.g. Andrews & McIntyre 1978; Bühler 2009, § 10). First, we define the linear particle displacement $\boldsymbol{\xi}$ as

$$\boldsymbol{\xi}_{,t} = \boldsymbol{u}^{(1)}, \tag{4.1}$$

$\boldsymbol{x} + \boldsymbol{\xi}(\boldsymbol{x}, t)$ thus being the linear position at time t of a material particle whose mean position is $\boldsymbol{x}$. Next, deriving the GLM equations partially consists of evaluating all fields at the displaced positions $\boldsymbol{x} + \boldsymbol{\xi}$:

$$\varphi(\boldsymbol{x}, t) \rightarrow \varphi^\xi(\boldsymbol{x}, t) = \varphi(\boldsymbol{x} + \boldsymbol{\xi}(\boldsymbol{x}, t), t) \tag{4.2}$$

and decomposing the quantities φ^ξ into Lagrangian-mean and Lagrangian-disturbance fields:

$$\varphi^\xi = \overline{\varphi}^L + \varphi^\ell, \tag{4.3}$$

where

$$\overline{\varphi}^L = \overline{\varphi^\xi} \quad \text{and therefore} \quad \overline{\varphi^\ell} = 0, \tag{4.4}$$

with $\overline{(\ )}^L$ called the GLM operator and $\overline{(\ )}$ denoting the Eulerian averaging operator. As said above, this average is performed over a fast time scale (say a few tidal cycles) in order to eliminate all $O(a)$ wave motions while retaining the slow evolution of the Lagrangian-mean flow. For the homogeneous background flow considered here we have that $\boldsymbol{u}^\ell = \boldsymbol{u}^{(1)}$ at $O(a)$ and Lagrangian disturbance and mean quantities scale as a and a^2, respectively, like their Eulerian counterparts.

The $O(a^2)$ GLM momentum equation, adapted from Bühler & McIntyre (1998, equation (9.4)), can be cast in the form

$$\left(\overline{\boldsymbol{u}}^L - \boldsymbol{p}\right)_{,t} + f\hat{\boldsymbol{z}} \times \overline{\boldsymbol{u}}^L - \overline{b}^L\hat{\boldsymbol{z}} = \overline{b^\ell \nabla \zeta} + \overline{\nabla(\ldots)}, \tag{4.5}$$

where $\boldsymbol{p} = -\sum_{j=1}^3 \overline{\left[u_j^\ell + (f/2)(\hat{\boldsymbol{z}} \times \boldsymbol{\xi})_j\right] \nabla \xi_j}$ is the Lagrangian pseudomomentum per unit mass, $\zeta = \boldsymbol{\xi} \cdot \hat{\boldsymbol{z}}$ and subscripts not preceded by commas denote Cartesian

components. The vector field $\boldsymbol{p}$ is a wave property whose time derivative vanishes owing to the assumed steadiness of the wave field and the dots in (4.5) refer to terms that will not play any role in the $O(a^2)$ GLM vorticity equation, which for $\boldsymbol{p}_{,t} = 0$ is

$$\nabla \times \overline{\boldsymbol{u}}^L_{,t} - f\overline{\boldsymbol{u}}^L_{,z} - \nabla \times (\overline{b}^L\hat{\boldsymbol{z}}) = \nabla \times (\overline{b^\ell \nabla \zeta}) = \boldsymbol{C}. \tag{4.6}$$

This omits a term $(\nabla \cdot \overline{\boldsymbol{u}}^L)f\hat{\boldsymbol{z}}$ on the left-hand side, which is justified because according to Andrews & McIntyre (1978, equation (9.4)), $\nabla \cdot \overline{\boldsymbol{u}}^L = (1/2)\partial[\sum_{j,k} \overline{(\xi_j\xi_k)}_{,jk}]/\partial t$ holds at $O(a^2)$ for incompressible flows and therefore

$$\nabla \cdot \overline{\boldsymbol{u}}^L = 0 \tag{4.7}$$

holds for stationary waves, which leads to (4.6). To complete our set of equations, the Lagrangian-mean and Lagrangian-disturbance equations for the buoyancy, adapted from Bühler & McIntyre (1998, equations (9.6) and (9.7)), are

$$\overline{b}^L_{,t} + N^2\overline{w}^L + \alpha^L\overline{b}^L = 0, \tag{4.8a}$$

$$b^\ell_{,t} + N^2w^\ell + \alpha b^\ell = 0. \tag{4.8b}$$

Note that in (4.8a), we introduce a new parameter α^L instead of simply setting $\alpha^L = \alpha$. The motivation for this is that we view the radiative damping in the linear equations as a crude model for turbulent dissipation, which is more likely to act preferentially on the sheared internal waves rather than on the smooth balanced flow. So, in order to keep room for future discussions, we leave the value of α^L a free parameter ranging between 0 and α.

Together, (4.6), (4.7) and (4.8a) form a complete set of Lagrangian-mean equations, which has the obvious advantage over its Eulerian-mean counterpart that there is only a single disturbance-induced forcing term on the right-hand side, namely the disturbance-buoyancy curl term $\boldsymbol{C}$ in (4.6). Also, the boundary conditions for the leading-order Lagrangian-mean flow are simply $\overline{w}^L = 0$ at both $z = H$ and $z = 0$, because the GLM theory preserves the impermeability of the mean boundary (Andrews & McIntyre 1978, §4.2). In contrast, the Eulerian boundary conditions for $\overline{w}$ are typically inhomogeneous at moving boundaries, owing to Stokes corrections, or lack thereof. This is another advantage of the Lagrangian formalism.

Now, as noticed by Bühler & McIntyre (1998), in the absence of dissipation $\overline{b^\ell \nabla \zeta}$ can be written in the form of a perfect gradient and its curl would then be zero in (4.6). This makes explicit that a stationary non-dissipating field of internal waves does not force the mean flow at leading order, which is an extension to three-dimensional mean flows of the classical results for zonally symmetric mean flows known under the general heading of 'non-acceleration results' (e.g. Andrews, Holton & Leovy 1987).

In our case, the presence of the dissipative term in (3.2b) provides the key forcing term for the GLM vorticity equation, which we now derive. Because $w^\ell = w^{(1)}$ and because (4.8b) and (3.2b) are identical, (3.4) holds for $\tilde{b}^\ell$ as well. Recalling (3.3), we find after an elementary computation that for monochromatic waves

$$\overline{b^\ell \nabla \zeta} = \nabla\overline{(\ldots)} + \boldsymbol{F}, \tag{4.9}$$

where dots refer to irrelevant potential terms and where

$$\boldsymbol{F} = \frac{\alpha N^2}{2(\omega^2 + \alpha^2)\omega}\text{Im}(\tilde{w}^*\nabla\tilde{w}). \tag{4.10}$$

This makes obvious that only $\boldsymbol{F}$, hereafter referred to as the effective mean force, will have an impact on the vorticity dynamics, while (4.10) once more shows that dissipation is essential in order to obtain a non-zero $\boldsymbol{F}$. Physically, the origin of $\boldsymbol{F}$ lies in vertical buoyancy forces b^ℓ that act on vertical displacements ζ in Kelvin's circulation theorem when applied to undulating material contours. This is the same physics as in the more familiar situation of zonal averaging. We note in passing that $-\boldsymbol{F}$ is also the dissipative term that would appear on the right-hand side of the evolution equation for the pseudomomentum vector $\boldsymbol{p}$; this is in accordance with the general relations between $\overline{Q}^L$, the Lagrangian-mean PV, and $\boldsymbol{p}$ in GLM theory (e.g. McIntyre & Norton 1990; Bühler 2000, 2009).

The curl of $\boldsymbol{F}$ turns out to be

$$\boldsymbol{C} = \boldsymbol{\nabla} \times \boldsymbol{F} = \boldsymbol{\nabla} \times (\overline{b^\ell \boldsymbol{\nabla} \zeta}) = \frac{\alpha N^2}{2(\omega^2 + \alpha^2)\omega} \frac{\boldsymbol{\nabla} \tilde{w}^* \times \boldsymbol{\nabla} \tilde{w}}{\mathrm{i}}, \qquad (4.11)$$

where it is noteworthy that $\boldsymbol{\nabla} \tilde{w}^* \times \boldsymbol{\nabla} \tilde{w}$ is either zero or purely imaginary.

Finally, (4.11) can be used to obtain an order-of-magnitude scaling for $\boldsymbol{C}$. In particular, the vertical component of $\boldsymbol{C}$ involves only horizontal derivatives of $\tilde{w}$, which scale with $1/L$, and $\tilde{w}$ itself scales with $U_0 h_0/L$. Combining this with the small parameters in (2.2) and the definition of the wave slope μ yields

$$C_z = \boldsymbol{C} \cdot \hat{z} \sim \frac{\alpha N^2}{2(\omega^2 + \alpha^2)\omega} \frac{U_0^2 h_0^2}{L^4} \approx \frac{\alpha}{\omega} \frac{\omega^2 - f^2}{2} a^2 \epsilon^2. \qquad (4.12)$$

The second form also uses $\alpha \ll \omega$ and $N \gg \omega$ for simplicity. This shows that C_z is very sensitive to the size of $U_0 h_0/L^2$.

4.3. *Potential vorticity evolution*

So far we have considered the complete mean-flow response, without distinguishing between strong and weak interactions. As said above, strong, resonant forcing of the mean flow due to a stationary wave field can be achieved only if the forcing $\boldsymbol{C}$ projects onto the PV evolution of the mean flow. In the present situation the $O(a^2)$ Lagrangian-mean PV relative to the unperturbed background flow can be written as (Bühler 2009)

$$\overline{Q}^L = \left[\boldsymbol{\nabla} \times \left(\overline{\boldsymbol{u}}^L - \boldsymbol{p} \right) \right] \cdot \hat{z} + \frac{f \overline{b}^L_{,z}}{N^2} + \frac{1}{2} f \sum_{j,k} \overline{(\xi_j \xi_k)}_{,jk}. \qquad (4.13)$$

The last term is due to a Lagrangian-mean divergence or density dilation effect; notably this term as well as the pseudomomentum term are both constant in time for a stationary wave field, so their time derivatives vanish.

In order to know how the PV evolves, we use the vertical component of (4.6) as well as (4.8*a*) and get

$$\overline{Q}^L_{,t} + \frac{\alpha^L f}{N^2} \overline{b}^L_{,z} = \boldsymbol{C} \cdot \hat{z} = C_z = \hat{z} \cdot (\boldsymbol{\nabla} \times \boldsymbol{F}). \qquad (4.14)$$

Clearly, the vertical curl of the horizontal components of $\boldsymbol{F}$ is the only part of the effective mean force that can produce a strong interaction. (We note in passing that we do not expect to see remote recoil effects (Bühler & McIntyre 2003) of the waves on the vortical motion, as the amplitude of the aforementioned flow would need to be two orders of magnitude higher in amplitude in order to appear at $O(a^2)$.)

	$\alpha^L = 0$	$\alpha^L \neq 0$
Two-dimensional case ($\partial/\partial x = 0$ or $\partial/\partial y = 0$)	Yes	Yes
Three-dimensional case	No	Yes[*]

TABLE 1. Is a steady state possible for the Lagrangian-mean flow? 'Yes[*]' means that the interior equations make a steady state possible but not generally compatible with the boundary conditions at the top and bottom of the domain. 'No' implies a secular growth of the Lagrangian-mean PV.

The damping term on the left-hand side might compensate the forcing term C_z, which would indicate a possible steady mean-flow response in forced–dissipative balance. Of course, whether or not this might occur also depends on our modelling choice for the parameter α^L. We will now investigate a few different scenarios in which the possible mean-flow evolutions can be studied in detail.

5. Bounded and unbounded mean-flow responses

In order to evaluate whether the mean flow can have a dynamical importance beyond $O(a^2)$, we now investigate when a bounded, steady mean-flow is possible and when not. We use the complete GLM equations, but also use the insight provided by the GLM PV equation. Several cases can be distinguished and the casual reader might want to skip to table 1, where the results are summarized.

5.1. *Two-dimensional case*

Let us first consider the two-dimensional case where $\partial/\partial y = 0$. In this case, $\nabla \tilde{w}$ and $\nabla \tilde{w}^*$ are in the (x, z) vertical plane. $\boldsymbol{C}$ is perpendicular to both vectors (cf. equation (4.11)), so we have $\boldsymbol{C} = C_y \hat{\boldsymbol{y}}$, implying that the PV equation (4.14) is unforced. Hence we expect that a steady state is possible.

Cancelling t- and y-derivatives in $((4.6) \cdot \hat{\boldsymbol{z}})$ yields $\overline{w}^L_{,z} = 0$ and hence $\overline{w}^L = 0$ from the boundary conditions. Similarly, the x-component of (4.6) together with (4.7) imply that $\overline{u}^L = 0$. Two cases can now be distinguished, depending on the value of α^L. If $\alpha^L = 0$ then equation $((4.6) \cdot \hat{\boldsymbol{y}})$ gives

$$-f\overline{v}^L_{,z} + \overline{b}^L_{,x} = C_y. \tag{5.1}$$

To obtain a unique steady state we need to exploit the fact that (4.14) tells us that $\overline{Q}^L$ keeps its initial value, which is zero provided we consider that the waves have been set up from a state of rest. In principle, by combining $\overline{Q}^L = 0$ and (5.1), it is possible to compute the detailed steady state provided one has expressions for the pseudomomentum and the other wave properties that appear in (4.6).

On the other hand, if $\alpha^L \neq 0$ then the situation is simpler because now (4.8a) together with $\overline{w}^L = 0$ implies $\overline{b}^L = 0$ and $\overline{v}^L$ then follows from

$$\overline{v}^L_{,z} = -C_y/f. \tag{5.2}$$

The only non-vanishing steady response of the wave forcing is therefore contained in a steady flow parallel to the ridge, which is coupled to the along-ridge forcing by rotation. Contrary to the case where $\alpha^L = 0$, the Lagrangian-mean isopycnals are horizontal.

Either way, it is worth noticing that the two-dimensional vertical slice model, widely used in practice owing to its reduced computational cost, does not allow any resonance between the effective mean force and the balanced mode, which results only in a weak, non-resonant response equilibrating at $O(a^2)$. However, one should note the potential caveat that the steady mean response that we computed here might in fact be unstable to oscillatory vacillations in a manner familiar in atmospheric science from the Plumb model of the quasi-biennial oscillation (e.g. Andrews *et al.* 1987).

5.2. *Three-dimensional case*

The general three-dimensional steady Lagrangian-mean vorticity and buoyancy equations are

$$-f\overline{u}_{,z}^{L} - \overline{b}_{,y}^{L} = C_x, \tag{5.3a}$$

$$-f\overline{v}_{,z}^{L} + \overline{b}_{,x}^{L} = C_y, \tag{5.3b}$$

$$-f\overline{w}_{,z}^{L} = C_z, \tag{5.3c}$$

$$N^2\overline{w}^{L} = -\alpha^{L}\overline{b}^{L}. \tag{5.3d}$$

Note that because $\nabla \cdot C = 0$ (cf. (4.11)), the Lagrangian-mean incompressibility condition is implicit in the above set of equations.

The interpretation of the above system of equations is the following. According to (5.3c), the mean-flow forcing induces a vertical Lagrangian-mean velocity. From here, two cases have to be distinguished: α^L vanishing or not vanishing.

If $\alpha^L \neq 0$ then the interior equations make a steady state possible, although a caveat regarding the bottom boundary condition arises. Indeed, (5.3d) shows that isopycnals bend. Equations (5.3a)–(5.3b) then show that the horizontal Lagrangian-mean velocities are forced by the horizontal components of C but also by C_z through $\overline{b}^{L}$ and $\overline{w}^{L}$. As mentioned in §4.2, the GLM theory preserves the impermeability of the boundaries and therefore, $\overline{w}^{L}|_{z=H} = 0$. Integrating (5.3c) over the fluid column therefore yields

$$\overline{w}^{L}\big|_{z=0} = \frac{1}{f} \int_0^H C_z(\boldsymbol{r}, z)\, \mathrm{d}z, \tag{5.4}$$

which has to be compatible with the bottom boundary condition:

$$\overline{w}^{L}\big|_{z=0} = 0. \tag{5.5}$$

Proving analytically that the steady state, deduced from the interior equations is never compatible with the boundary conditions, is daunting and not attempted here. However, we will see in §6.3 an example of a configuration where (5.4) and (5.5) obviously contradict each other, a fact one has to be aware of when investigating different situations. The conclusions one can draw are multiple and possibly mutually exclusive: one could deduce that a steady state is unlikely to exist but also that a top and/or a bottom boundary layer(s) unaccounted for in our model can develop.

If $\alpha^L = 0$, on the other hand, an inconsistency between (5.3a) and (5.3d) arises and the assumption that a steady state is possible has to be abandoned. In this case, (4.14) becomes

$$\overline{Q}_{,t}^{L} = C_z. \tag{5.6}$$

The PV then grows secularly until the asymptotic ordering, on which our model is based, is violated. A conclusion we can draw from comparing all two- and three-dimensional cases is that the possibility of the mean flow reaching a steady state or not depends greatly on the configuration; our findings are summarized in table 1. Clearly, strong, resonant responses of the mean flow can only be found in three-dimensional configurations.

5.3. *Time scale for significant PV growth*

We should say a few words about the magnitude of C_z, so we must first associate its magnitude with a meaningful metric. One natural approach to this in the case of unbounded growth of $\overline{Q}^L$ is to compute the time scale over which $\overline{Q}^L$ would grow to a magnitude such that the neglected horizontal advection term $\left(\overline{u}^L \cdot \nabla_H\right)\overline{Q}^L$ in (5.6) becomes important. A simple estimate for this follows from the growth implied by (5.6), namely that $\overline{Q}^L = C_z t$ plus some $O(a^2)$ initial condition. The horizontal Lagrangian-mean velocity signal associated with this growing PV disturbance would scale as $\overline{u}^L \sim \overline{Q}^L L$ with the common horizontal length scale L. Hence the nonlinear term becomes comparable to the forcing term at a time t such that

$$\left(\overline{u}^L \cdot \nabla_H\right)\overline{Q}^L \sim C_z \quad \Rightarrow \quad \left(\overline{Q}^L\right)^2 \sim C_z \quad \Rightarrow \quad t^2 C_z \sim 1. \tag{5.7}$$

Presumably, then, the linear growth of $\overline{Q}^L$ saturates over a time scale

$$T = \frac{1}{\sqrt{C_z}} \quad \text{and} \quad \overline{Q}^L = C_z T = \sqrt{C_z} \tag{5.8}$$

is the magnitude of the PV disturbance that has been reached at this saturation time.

6. Numerical calculations in three dimensions

We now focus our attention on the horizontal effective force, hereafter referred to as $\boldsymbol{F}_H$, which is the only one acting on the PV, and the forcing term C_z. We compute these quantities numerically in a few cases.

6.1. *Numerical procedure*

Because we are considering a finite-extent topography, Fourier transforms are not an efficient way of computing the convolution in (3.18). They must, rather, be calculated at each location, point by point, which is very costly from a numerical point of view.

We choose an axisymmetric Gaussian seamount, for simplicity reasons but also because it allows us to design a faster way of computing C_z. First, it makes it more useful to switch to a polar coordinate system (r, θ, z) defined by $(x, y) = r(\cos\theta, \sin\theta)$ centred on the seamount, whose bathymetry is given by

$$h(r) = h_0 \exp\left(-\frac{r^2}{2L^2}\right), \tag{6.1}$$

which implies

$$\tilde{w}_0(r, \theta) = -\frac{U_0 h_0}{L^2} r \exp\left(-\frac{r^2}{2L^2}\right)(\cos\theta + i\gamma\sin\theta). \tag{6.2}$$

In the new coordinate system and for a Gaussian topography, $\tilde{w}$ becomes (cf. appendix B):

$$w = W(r, z)(\cos\theta + i\gamma \sin\theta), \tag{6.3}$$

with

$$W(r, z)$$
$$= -\frac{U_0 h_0}{L^2} r \exp\left(-\frac{r^2}{2L^2}\right) \left\{ 1 - \frac{z}{H} - \frac{2}{\pi} \sum_{m=1}^{\infty} \frac{\sin(k_m z)}{m} + \frac{\pi(\mu\beta)^2}{iHr} \int_0^{\infty} r_0 \exp\left(-\frac{r_0^2}{2L^2}\right) \right.$$
$$\left. \times \left[r I_0\left(\frac{rr_0}{L^2}\right) - r_0 I_1\left(\frac{rr_0}{L^2}\right) \right] \left[\sum_{m=1}^{\infty} k_m H_0^{(1)}(\mu\beta k_m r_0) \sin(k_m z) \right] dr_0 \right\}, \tag{6.4}$$

where I_n is the order-n modified Bessel function of the first kind. Hence, instead of computing the $\mathscr{C}_m$ functions, which involve two-dimensional convolutions, the computation of $\tilde{w}$ can be reduced to the computation of W, which involves only one integral. Including the dependence on θ is then straightforward, as shown by (6.3).

All quantities displayed here are calculated on a grid of finite extent and up to a vertical mode number M. In all cases, we choose $M = 32$ and check that the highest vertical mode computed has a negligible amplitude compared to the few dominant modes.

Sufficient horizontal resolution is required in order for the integration, present in the expression of $W(r, z)$ and computed with the trapezoidal method for each discrete r, to give physical values. Empirical trials indicate that resolving the horizontal wavelength of the highest mode by 16 points gives satisfactory results.

The radial extent R of the domain is chosen to be large enough for the numerical integrations to be good approximations of integrals whose endpoints go to infinity. We choose $R = 4H/\mu \approx 160$ km $\approx 16L$. Finally, we choose a fairly weak dissipation rate (discussed in §6.4)

$$\frac{\alpha}{\omega} = 0.1 \tag{6.5}$$

and note that the other numerical values are defined in §2.1. An illustration of $\text{Re}(\tilde{w})$ for $\gamma = 0$ is presented in figure 2.

Note that unlike in the model of Pétrélis *et al.* (2006), the numerical solutions we will compute next do not exhibit small-scale noise for the resolutions we use. This is due to the second part of (3.17).

6.2. *Rectilinear tide*

We first investigate the case $\gamma = 0$, for which (4.10), (4.11) and (6.3) yield

$$\boldsymbol{F}_H = \begin{pmatrix} F_r \\ F_\theta \end{pmatrix} = \frac{\alpha N^2}{2(\omega^2 + \alpha^2)\omega} \begin{pmatrix} \text{Im}(W^* W_{,r})\cos^2\theta \\ 0 \end{pmatrix}, \tag{6.6}$$

$$C_z = C_z^I(r, \theta, z) = \frac{\alpha N^2}{2(\omega^2 + \alpha^2)\omega} \frac{\text{Im}(W^* W_{,r})}{r} \sin(2\theta). \tag{6.7}$$

The horizontal effective force $\boldsymbol{F}_H$ has no azimuthal component and its radial component has two maxima, aligned with the direction of the tide. This yields a quadrupolar pattern for C_z^I, as seen on figure 3. The quadrupolar nature of the PV forcing pattern is consistent with expectations based on simple wave-packet thinking.
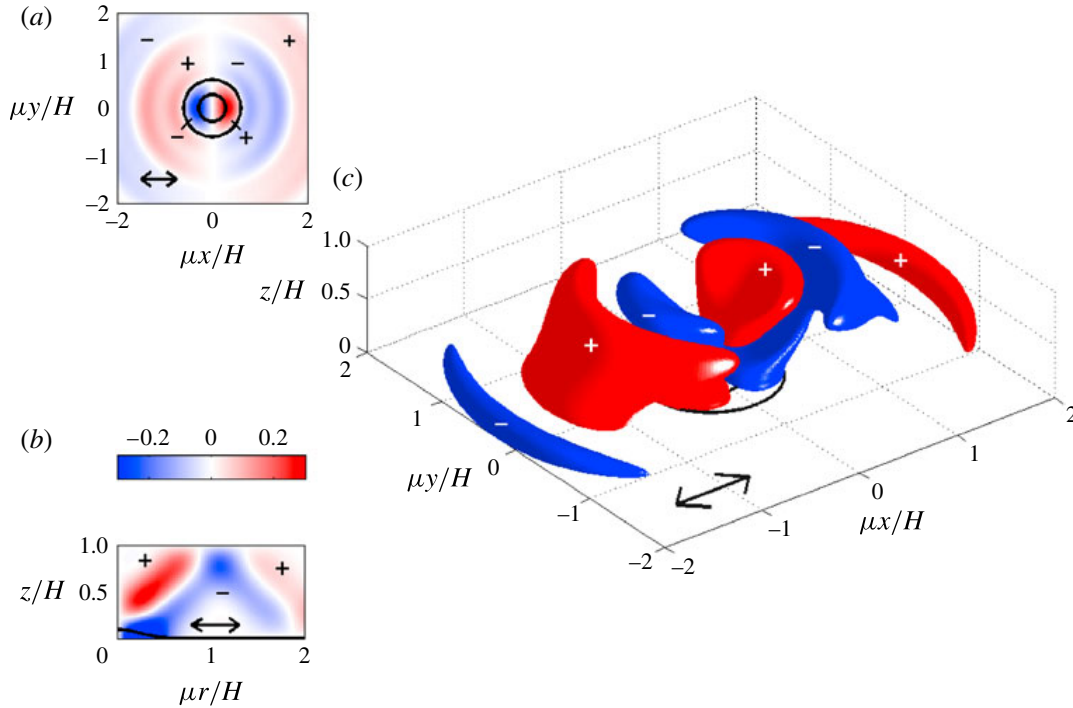
FIGURE 2. (Colour online) $\mathrm{Re}(\tilde{w})/(a\mu U_0)$ for $\gamma = 0$. Axes are stretched so that waves seem to propagate vertically at angle $45°$. (*a,b*) horizontal and vertical slices at $z = H/2$ and $\theta = 0$, respectively (the colour scale applies to both). (*c*) Three-dimensional isocontours marking the loci where $|\tilde{w}|/(a\mu U_0) = 0.1$. Blue is for negative values, red for positive, as indicated by the plus and minus signs. In all three pictures, the double arrow marks the direction of the barotropic tide. In (*a,c*), the inner and outer black circles indicate the topographic isocontours $h = h_0/2$ and $h = h_0/20$, respectively. In (*b*), the solid line corresponds to the topography height multiplied by 4 for purposes of visualization.

For example, as described by e.g. Bretherton (1969) and Bühler (2010), the dissipation of a slowly varying wave packet crossing an isopycnal surface generates a dipolar PV forcing pattern on that isopycnal. In our case, the forcing is now an oscillating tide, leading to waves that are radiated mainly in two opposite directions and the PV response is qualitatively in the form of two dipoles whose PV distributions nearly cancel, i.e. a quadrupole. Another way of seeing the same phenomenon is to note that a quadrupolar PV forcing pattern is a horizontal derivative of a dipolar pattern in $\boldsymbol{F}_H$, and the spatial integral of such a dipolar $\boldsymbol{F}_H$ is zero. This is consistent with a zero mean drag force on the topography over a full tidal oscillation cycle. This is unlike the mountain lee-wave scenario, where there is a non-zero drag force on the mountain and a corresponding equal-and-opposite net effective mean force on the fluid, which is felt where the waves dissipate. So for lee waves one expects a dipolar PV forcing pattern and for tidal waves one expects a quadrupolar pattern.

In this example the numerical magnitude of C_z^I is $\sim 2 \times 10^{-6} \times a U_0 \omega / L \approx 4 \times 10^{-17}\ \mathrm{s}^{-2}$. Using the estimate (5.8) for the time until horizontal advection becomes important then yields $T \approx 5$ years, which is very long compared to the tidal cycle. If U_0 and h_0 were both doubled then by (4.12) the value of C_z would increase by a factor of 16 whilst that of T would decrease by a factor of 4. Still, it seems that one can safely assume that many tidal cycles will pass before the wave-induced PV disturbance can no longer be described by our theory.
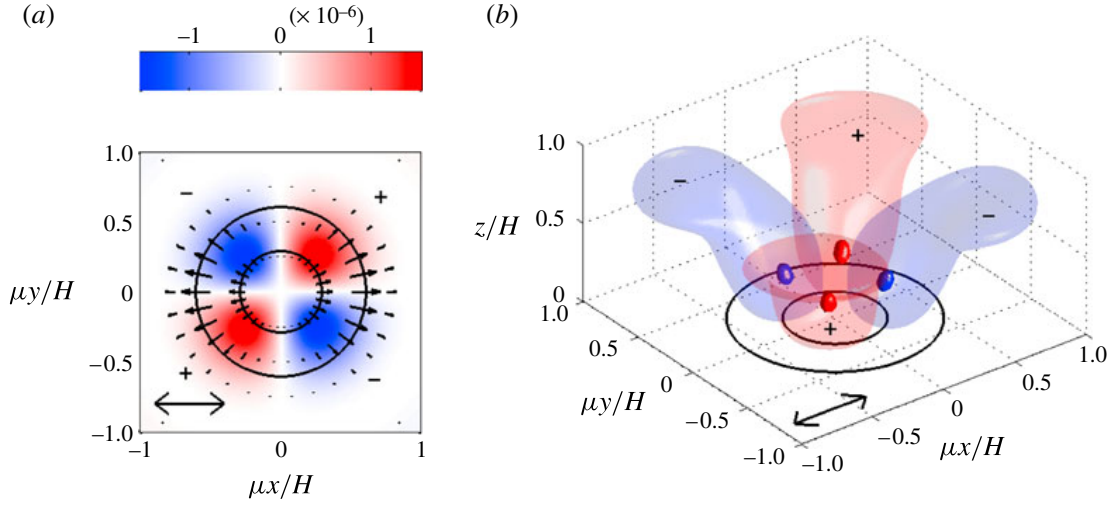
FIGURE 3. (Colour online) $C_z^I L/(aU_0\omega)$, which corresponds to the same computation as for figure 2. For explanations of the double arrows, the black lines and the plus and minus signs, see figure 2. (a) A horizontal slice located at altitude $z = H/2$. Single arrows correspond to $\boldsymbol{F_H}$, their scale being arbitrary. (b) The inner dark and outer light isocontours show the loci of $|C_z^I|L/(aU_0\omega) = 2.4 \times 10^{-6}$ and 0.4×10^{-6}, respectively $(\max[C_z^I L/(aU_0\omega)] \approx 2.7 \times 10^{-6})$.

6.3. *Rotary tide*

We now consider $\gamma \neq 0$, which consists of adding to the previous tide a transverse component, in time quadrature with the former. Using again (4.10) and (6.3), we now have

$$\boldsymbol{F_H} = \frac{\alpha N^2}{2(\omega^2 + \alpha^2)\omega} \begin{pmatrix} \mathrm{Im}(W^* W_{,r})(\cos^2\theta + \gamma^2\sin^2\theta) \\ \gamma \, |W|^2 \, /r \end{pmatrix}. \tag{6.8}$$

Important qualitative differences arise compared to the $\gamma = 0$ case, as the effective force is now the sum of three contributions: in F_r, the contribution of the previous, along-$\hat{\boldsymbol{x}}$ rectilinear tide proportional to $\cos^2\theta$ and the individual contribution of the transverse, along-$\hat{\boldsymbol{y}}$ component proportional to $\sin^2\theta$; in F_θ, a cross-term blending contributions from both tidal components and responsible for a non-zero azimuthal component of the effective force.

Other consequences of allowing some ellipticity for the rotary barotropic tide are made apparent in the PV forcing, again with the help of (4.11):

$$C_z = (1 - \gamma^2)C_z^I(r, \theta, z) + \gamma C_z^X(r, z), \quad \text{with } C_z^X(r, z) = \frac{\alpha N^2}{(\omega^2 + \alpha^2)\omega} \frac{\mathrm{Re}(W^* W_{,r})}{r}. \tag{6.9}$$

The contributions of each one of the along-$\hat{\boldsymbol{x}}$ and along-$\hat{\boldsymbol{y}}$ tidal components, shaped as quadrupoles such as the one displayed in figure 3, are now contained in $(1 - \gamma^2)C_z^I$. Besides their magnitudes differing by a factor γ^2, the two patterns of each individual component are 90° of horizontal rotation from each other around the central vertical axis and because they are quadrupolar, they are of opposite sign. The two contributions therefore cancel each other partially for $0 < |\gamma| < 1$ and completely for $|\gamma| = 1$.

On the other hand, the cross-term γC_z^X is independent of θ, as is F_θ. As can be seen on figure 4, F_θ has its maximum on the slope of the seamount, at a certain distance from its top and approximately (although not exactly) where C_z^X vanishes.
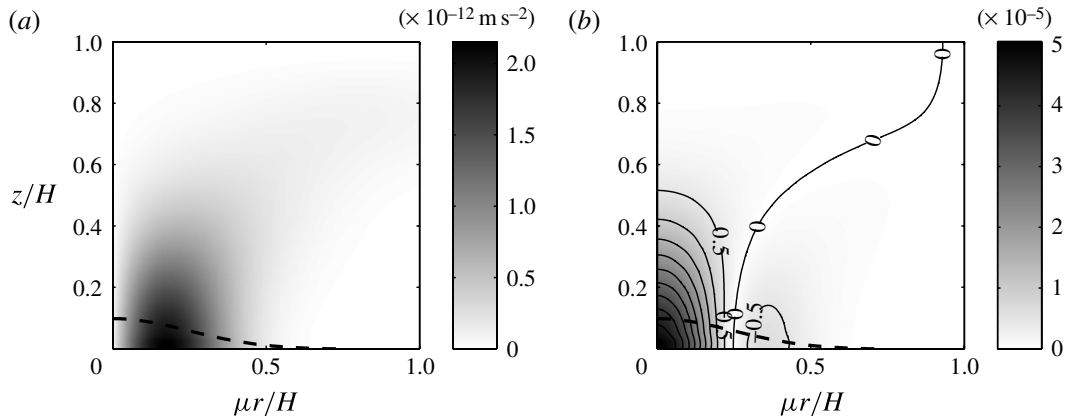
FIGURE 4. Cross-terms forcing the balanced flow in the case where $\gamma \neq 0$: (a) F_θ/γ and (b) $C_x^X L/(aU_0\omega)$. In (b), the grey scale corresponds to absolute values and contours correspond to algebraic values, with the -5×10^{-6}, 0 and 5×10^{-6} values marked explicitly. The dashed lines in (a) and (b) correspond to the topography height multiplied by 4 for purposes of visualization.
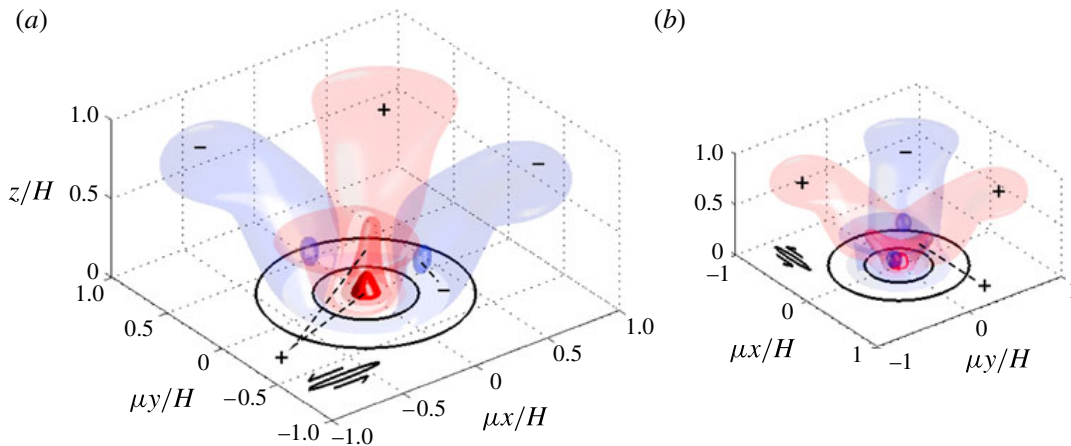

FIGURE 5. (Colour online) (a) As figure 3(b) but for $\gamma = 0.1$. The two outermost isocontours correspond to the same values as in figure 3, whereas the innermost isocontour corresponds to $C_z L/(aU_0\omega) = 4 \times 10^{-6}$ ($\max[C_z L/(aU_0\omega)] \approx 5.0 \times 10^{-6}$). The tidal double arrow of figure 3 has turned into a counterclockwise tidal ellipse of aspect ratio γ. (b) As (a) but with viewpoint rotated by 90° in the horizontal.

These elements suggest that the cross-terms are forcing a bottom-intensified vortex associated with (counter-)clockwise displacements around the seamount for $\gamma < 0$ ($\gamma > 0$). We note in passing that computations in Cartesian domains with elliptic instead of axisymmetric seamounts (not shown) show that the vortex shape actually follows the isobath contours.

To sum up, increasing ellipticity in the rotary barotropic tide decreases the magnitude of the original quadrupolar pattern derived in § 6.2 and increases the forcing of a bottom-intensified vortex, as illustrated in figures 5 and 6 for $\gamma = 0.1$ and 0.7. The former shows that even a modest value of γ induces a significant qualitative modification of C_z near the top of the mountain, while the latter shows how a strong

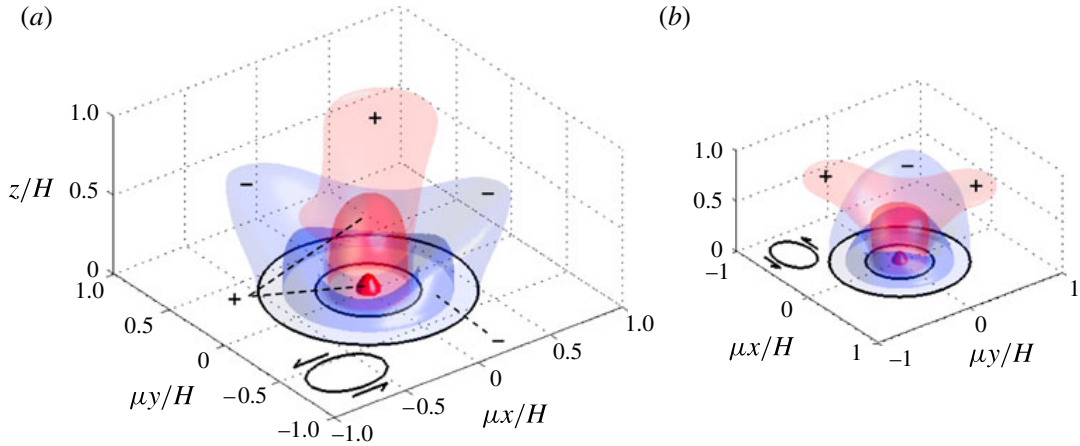(*a*)   (*b*)

FIGURE 6. (Colour online) As figure 5 but for $\gamma = 0.7$, and the innermost isocontour now corresponds to $C_z L/(aU_0\omega) = 30 \times 10^{-6}$ ($\max[C_z L/(aU_0\omega)] \approx 35 \times 10^{-6}$).

but realistic (cf. e.g. St Laurent & Garrett 2002) value of γ dramatically changes the PV forcing. The most striking consequence of increasing γ on the PV forcing is the amount that its spatial distribution is modified, becoming more confined to the vicinity of the topography, among other changes. Also, the magnitude of C_z increases sharply with γ: taking the values computed in §6.2 for $\gamma = 0$ as a reference, its maximum value is doubled for $\gamma = 0.1$ (cf. figure 5) and multiplied by 14 for $\gamma = 0.7$ (cf. figure 6).

6.4. *Influence of the dissipation*

The value of α that we have used so far, associated with a decay scale of about a week, is not wildly unreasonable but does not pretend to be realistic and is not deduced from the literature. Let us now briefly describe how the forcing of the mean flow is modified by variations of α.

Figure 7 shows the $\gamma = 0$ and 0.7 cases, for which $\alpha/\omega = 0.5$ (instead of the previous $\alpha/\omega = 0.1$). The peak values of C_z are now higher than their low-dissipation counterparts of §§6.2 and 6.3, while the low values of C_z occupy roughly the same volume, corresponding to a more rapid spatial decrease of the mean flow forcing.

Increasing the value of α has the effect of limiting the range of propagation of the $O(a)$ linear waves by increasing their dissipation near the topography. Hence, one can understand why the forcing of the mean flow increases in terms of peak value but that this increase is limited to the vicinity of the topography. Far from it, the amplitude of the wave field is reduced, as is the forcing of the mean flow.

6.5. *An example of focusing topography*

We have considered so far topography whose isobaths are convex. Bühler & Muller (2007) showed that topographies with concave isobaths could be interesting cases as they could induce three-dimensional focusing of internal waves far from the topography and hence enhanced wave breaking in those regions.

In order to model a concave topography, we create a horseshoe-shaped topography defined as

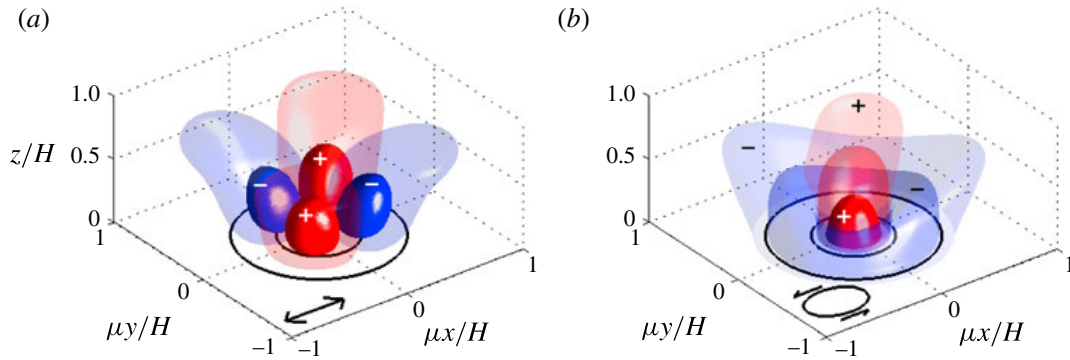$$h(r,\theta) = h_0 \exp\left(-\frac{(r-\sigma)^2}{2L^2}\right) \cos^2\left(\frac{\theta}{2}\right), \qquad (6.10)$$

FIGURE 7. (Colour online) Two cases for which the linear dissipation rate per unit time α is increased from $\omega/10$ to $\omega/2$. (*a*) As figure 3, with the exception that $\max[C_z L/(a U_0 \omega)] \approx 5.9 \times 10^{-6}$. (*b*) As figure 6(*a*), with the exception that $\max[C_z L/(a U_0 \omega)] \approx 140 \times 10^{-6}$.

where σ is the distance from the crest of the ridge to the centre of the domain and the opening along the $x < 0$ axis is an attempt to model a topographic feature more plausible than an annulus, resembling a submarine cirque or the mouth of a submarine canyon. All previous numerical values are kept and we define $\sigma = 3L$.

In this configuration, the dependence on θ of $\tilde{w}(r, \theta, z)$ is less straightforward than for the axisymmetric topography and instead the computations are done on a square Cartesian grid. Owing to the increased computational cost of this procedure, the lateral extent of the semi-domain (equivalent to R in our case) is reduced to $2H/\mu$ and the number of computed modes is reduced to $M = 16$. All other parameters, namely α, the horizontal resolution and all numerical values of the other physical parameters are kept the same. As a result, the computed C_z is somewhat more noisy, which does not do any harm to the qualitative conclusions we want to draw. More problematic is the presence of extra artificial noise along the central fluid column, near the bottom. This is due to the singularity of the topography gradients in $r = 0$ and is only significant if $\gamma \neq 0$. We therefore set to zero the values of C_z around the origin of the domain in the $\gamma = 0.7$ case we study next, which again does not change our qualitative conclusions.

Figures 8 and 9 show that whether $\gamma = 0$ or $\gamma = 0.7$, C_z peaks around the centre of the topography and high above it, where the wave beams converge, therefore agreeing with the results of Bühler & Muller (2007). Note that for $\gamma = 0$, the quadrupolar pattern has virtually disappeared because of the asymmetry of the topography. Such focusing topographies could give insights into cases with seamounts with supercritical slopes, for which wave beams can focus above the summit in a similar way (e.g. Carter, Gregg & Merrifield 2006).

6.6. *Comparison with other mean flows around topographies*

A clear conceptual distinction exists between our model and other observations, such as boundary-layer effects or tidal rectification. Unfortunately, they are likely to be confused with each other in a realistic context, as they seem to produce mean flows with qualitatively similar features.

To our knowledge, the case presented in §6.2 of a rectilinear tidal forcing with an axisymmetric mountain has been studied in only a few cases, and only with supercritical slopes. For example, mean flows at second order in wave amplitude have been reported in the laboratory experiments and numerical simulations of King, Zhang & Swinney (2009). However, these mean flows involve significant vertical motion and
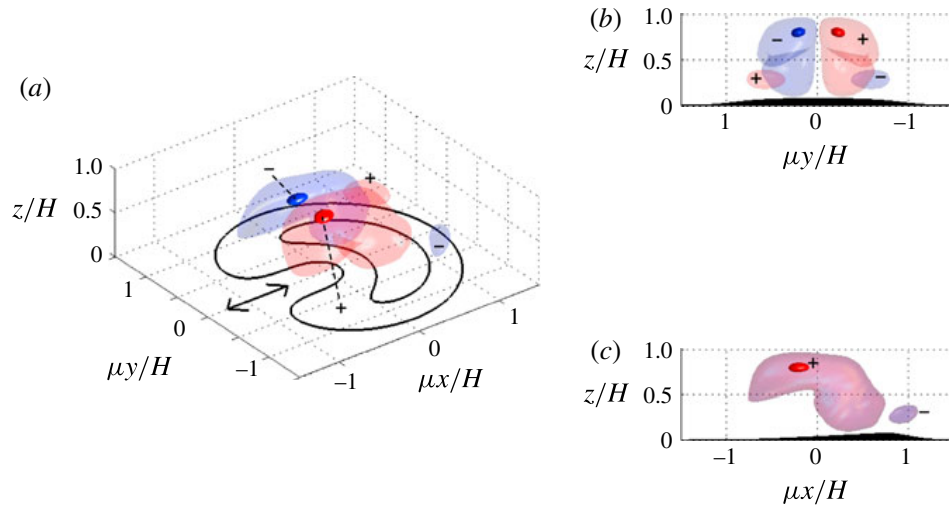
FIGURE 8. (Colour online) (*a*) $C_z L/(a U_0 \omega)$ in the case of a horseshoe topography and $\gamma = 0$. Double arrows, black lines and plus and minus signs have the same definitions as in figure 2. The inner dark and outer light isocontours show the loci of $|C_z| L/(a U_0 \omega) = 8 \times 10^{-6}$ and 1×10^{-6}, respectively ($\max[C_z L/(a U_0 \omega)] \approx 9.2 \times 10^{-6}$). (*b*) The same object viewed from a location on the $(x < 0, y = 0)$ axis and (*c*) from a location on the $(x = 0, y < 0)$ axis. In (*b,c*), the topography is filled in black and its height is multiplied by 3 for purposes of visualization.
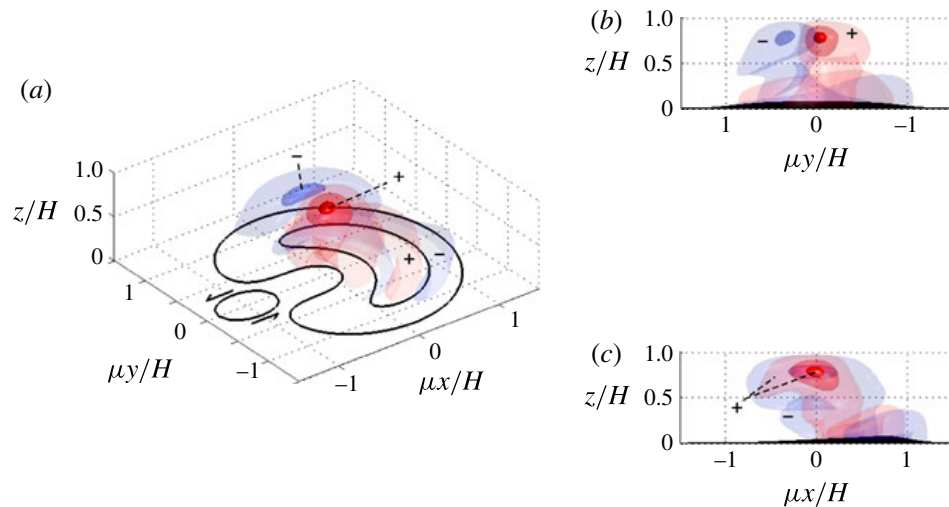

FIGURE 9. (Colour online) As figure 8 but for $\gamma = 0.7$. The black ellipse has the same definition as in figure 5. The two outermost isocontours show the same loci as in figure 8, whereas the innermost contour shows the locus of $|C_z| L/(a U_0 \omega) = 18 \times 10^{-6}$ ($\max[C_z L/(a U_0 \omega)] \approx 29 \times 10^{-6}$).

strong interactions with a viscous boundary layer, so they seem to be of a different kind than the balanced mean flows we have studied here.

Regarding the case with a rotary tide, at first sight, the forcing of bottom-intensified vortices in §6.3 appears reminiscent of either Taylor–Proudman dynamics or tidal

rectification (i.e. so-called residual currents). The first class of phenomena can readily be ruled out as the PV anomaly forcing is not fixed as cyclonic or anticyclonic, but, rather, depends on the sign of γ. Still, the question remains of whether our model is a reinterpretation of tidal rectification or whether it is a phenomenon of a different nature. We believe the latter is the case, and so we explain in the next paragraphs how 'tidal rectification' and 'residual currents' in the literature describe phenomena that do not include our model.

Tidal rectification has been studied in the shallow-water case by e.g. Huthnance (1973) and Loder (1980) and extended to the stratified case by Maas & Zimmerman (1989*a*,*b*). In the shallow-water case, Zimmerman (1981) provides a useful interpretation in terms of vorticity dynamics of how residual currents are generated: when flowing above topographies, boundary friction and Coriolis accelerations produce torques on the fluid columns which, integrated over tidal periods, provide a steady forcing on, say, the circulation around a seamount. In the uniformly stratified case, Maas & Zimmerman (1989*a*,*b*) identify the residual current as the zero-frequency harmonic component, arising when $\epsilon = O(1)$ or larger (cf. §2.2).

Both cases only necessitate studying the interaction of the barotropic tide with itself to generate mean flows. On the contrary, in our case, the barotropic tide and the mean-flow generation are different by two orders in asymptotic expansion, linear internal waves providing the link at the intermediate order. For example, if we were to transpose the mechanism we are describing in the present study to the configuration studied by Maas & Zimmerman (1989*a*,*b*), we would study nonlinear interactions between all wave harmonics. Extending the analogy even further, a similar study in a shallow-water configuration would investigate mean flows generated by dissipative shallow-water waves generated by the tide–topography system, whereas shallow-water tidal rectification consists of mean flows generated directly and locally by boundary friction in the the tide–topography system.

Whether our wave–mean model dominates over tidal rectification is determined by the excursion parameter ϵ. Assuming $\epsilon \ll 1$ places us in a case Maas & Zimmerman (1989*a*) call the 'deep-sea regime', for which advection by the barotropic tide and hence the residual currents become negligible, and for which our model dominates the forcing of the mean flow. On the other hand, as first noticed by Zimmerman (1978), problems of tidal rectification involve regimes for which $\epsilon = O(1)$, a regime Maas & Zimmerman (1989*a*) call the 'continental shelf regime'. As long as the topographic slopes are gentle, our mean-flow forcing will still happen at $O(a^2)$, whereas tidal rectification will be an $O(1)$ effect and will therefore dominate.

In regions where tidal excursion is strong, slopes are steep ($\epsilon, a = O(1)$) and mean flows are observed, it could be difficult to determine how much of the aforementioned mean flow is driven by dissipating internal waves or by tidal rectification, because both mechanisms could be at work (although, strictly speaking, the former would not be described by our weakly nonlinear theory). Unfortunately, our model does not provide any obvious way to solve this puzzle and case-by-case studies would have to be done. In view of these comments, it might be worthwhile to reassess the interpretations of some of the observations made in the past in the light of our new model. For example, Kunze & Toole (1997) describe observations of mean flows around Fieberling Guyot which could not be related to Taylor–Proudman dynamics, but for which the role of tidal rectification could not be clearly evaluated. Our model might provide a useful conceptual framework to reinterpret these data.

7. Concluding comments

Our main theoretical result is the derivation of the wave-induced effective force $\boldsymbol{F}$ in (4.10) and of its curl $\boldsymbol{C}$ in (4.11), which we repeat here for convenience:

$$\boldsymbol{C} = \boldsymbol{\nabla} \times \boldsymbol{F} = \boldsymbol{\nabla} \times (\overline{b^\ell \boldsymbol{\nabla} \zeta}) = \frac{\alpha N^2}{2(\omega^2 + \alpha^2)\omega} \frac{\boldsymbol{\nabla} \tilde{w}^* \times \boldsymbol{\nabla} \tilde{w}}{\mathrm{i}}. \tag{7.1}$$

The effective force $\boldsymbol{F}$ differs from $\overline{b^\ell \boldsymbol{\nabla} \zeta}$ by an irrotational gradient term, which does not affect $\boldsymbol{C}$. Physically, this irrotational gradient term is balanced by a mean pressure field and therefore does not lead to accelerations of the mean flow.

For a stationary wave field the force curl $\boldsymbol{C}$ comprises the entire effect of the dissipating waves on the mean flow and its vertical component C_z comprises the entire effect on the Lagrangian-mean PV. The final form in (7.1) depends on the specific wave problem we have investigated, but the form $\boldsymbol{C} = \boldsymbol{\nabla} \times (\overline{b^\ell \boldsymbol{\nabla} \zeta})$ holds generally for stationary wave fields subject to damping in the buoyancy field. As the vertical displacement ζ can be found from $\zeta_{,t} = w^{(1)}$ and as b^ℓ can be approximated by $b^{(1)}$, it seems that (7.1) could be used for diagnosing numerical simulations or observational data for fairly general stationary wave fields subject to buoyancy damping.

Of course, a more complete formulation would allow for dissipative terms in the momentum equation as well. As shown in Bühler (2000), such dissipative terms in the momentum equations add naturally to $\boldsymbol{F}$ provided that these terms are momentum-conserving in an integral sense (i.e. they derive from the divergence of a dissipative momentum flux tensor in the usual way). This includes the usual viscous Navier–Stokes terms but excludes Rayleigh damping, for example. Specifically, if a momentum-conserving force $\boldsymbol{D}$ were added to the momentum equations then one would need to add $\sum_j \overline{\xi_{j,i} D_j^\ell}$ to the ith component of $\boldsymbol{F}$ (e.g. Bühler 2009, §§ 11.1–11.1.1), i.e.

$$F_i = \overline{b^\ell \zeta_{,i}} + \sum_{j=1}^{3} \overline{\xi_{j,i} D_j^\ell} + \overline{(\ldots)_{,i}}. \tag{7.2}$$

This is the most general effective-mean-force formula for the Boussinesq system.

Now, one obvious extension of our specific wave problem would be to allow for finite tidal excursion, which corresponds to allowing the parameter ϵ to take large values. As is well known, for the linear dynamics this would produce a polychromatic wave field containing all harmonics of the tidal frequency, with amplitudes generally decreasing with the order of the harmonic. However, as far as the effective mean force is concerned, only quadratic combinations with zero frequency matter, which rules out any correlations between different harmonics. Hence the final term in (7.1) would simply be replaced by a sum over all the harmonics. So, it seems that extending our theory to finite excursion length would not lead to fundamentally new results.

To some extent the same could be said if one lifted the restriction to small topography amplitude and considered large topography features, simply because (7.1) is a local statement that does not depend on where and how the waves have been generated. So, while a three-dimensional numerical wave computation with finite-amplitude topography would certainly be more complicated owing to the possibility of critical topography slopes as well as the need to apply the boundary conditions at $z = h$ instead of $z = 0$, it would seem that the computation of the effective mean force and its curl would proceed just as in our very simple example. Still, with such extensions in place it would be interesting to investigate the mean-flow forcing in

realistic settings, such as the aforementioned Fieberling seamount discussed in Kunze & Toole (1997), for example. In such a case, the supercritical topography allows for beams to propagate upwards and radially inwards. Hence, one might expect to see mean-flow forcing patterns, reminiscent of the patterns described in § 6.5. As discussed in § 6.6 however, competition with tidal rectification would make it not trivial to interpret the results.

It is interesting to speculate on the long-time behaviour of the mean flow under the PV forcing induced by C_z. After all, the tides are at work relentlessly and there is no shortage of time for effects to accumulate. It seems reasonable to expect that the horizontal advection terms that have been neglected in (4.14) will eventually lead to self-advection of the PV field away from the forcing region; such behaviour is indeed known to occur in simpler shallow-water models for vortices generated by breaking waves on beaches (e.g. Bühler & Jacobson 2001; Barreiro & Bühler 2008). As argued before, in such a scenario the PV will saturate over a time scale proportional to $1/\sqrt{C_z}$ and at an amplitude scaling with $\sqrt{C_z}$, which from (7.1) and the definition of the wave slope μ would indicate that the PV amplitude scales as $\sqrt{\alpha(\omega^2 - f^2)/\omega}$ times the root-mean-square value of $\zeta_{,z}$. The latter is the non-dimensional amplitude of the waves and can therefore be expected to be of order unity for breaking waves. Hence one can estimate that the saturated PV amplitude should scale as $\sqrt{\alpha(\omega^2 - f^2)/\omega}$.

Finally, it would be very interesting to see via numerical simulation of the fully nonlinear system whether these saturation estimates for the PV are viable or not. However, as noted before, such simulations would have to be three-dimensional in order to capture this kind of secularly growing PV dynamics, which is entirely absent in two-dimensional models, and a configuration keeping a and ϵ small would have to be integrated for years before reaching saturation. At present, this perhaps makes such simulations prohibitively expensive.

Appendix A. Linear vertical velocity in two dimensions

We are looking for a solution of (3.5) in two dimensions ($\partial/\partial y = 0$), using the same approach as in § 3.2. We are now solving for $G(x, z; x_0)$:

$$G_{,xx} - (\mu\beta)^2 G_{,zz} = 0 \quad \text{for } (x, z) \neq (x_0, 0), \tag{A 1a}$$

$$G|_{z=H} = 0; \quad G|_{z=0} = \delta(x - x_0), \tag{A 1b}$$

and proceed to the same decomposition of G that lead to (3.9):

$$G(x, z; x_0) = \mathscr{G}(x, z; x_0) + \left(1 - \frac{z}{H}\right)\delta(x - x_0). \tag{A 2}$$

We then reproduce the series of operations spanning from (3.10) to (3.12) for which we now have to solve for each $\mathscr{G}_m$ an inhomogeneous *one*-dimensional Helmholtz

equation of wavenumber $\mu\beta k_m$, whose Green's function is

$$g_m(x; x_1) = \frac{\exp(i\mu\beta k_m|x - x_1|)}{2i\mu\beta k_m}. \tag{A 3}$$

Integrating over $\mathbb{R}$ instead of $\mathbb{R}^2$, we get the the equivalent of (3.15):

$$\mathscr{G}_m(x; x_0) = -\frac{2}{\pi m} g_{m,xx}(x; x_0) = \frac{\mu\beta}{iH} \exp(i\mu\beta k_m|x - x_0|) - \frac{2}{\pi m}\delta(x - x_0), \tag{A 4}$$

the final expression for $\mathscr{G}_m$ having been obtained using the one-dimensional Helmholtz equation that g_m is a Green's function of. The final expression for G is therefore

$$G(x, z; x_0) = \frac{\mu\beta}{iH} \sum_{m=1}^{\infty} \exp(i\mu\beta k_m|x - x_0|) \sin(k_m z)$$

$$+ \left(1 - \frac{z}{H} - \frac{2}{\pi} \sum_{m=1}^{\infty} \frac{\sin(k_m z)}{m}\right)\delta(x - x_0), \tag{A 5}$$

which yields (3.19) and (3.20).

Appendix B. Linear vertical velocity expressed in polar coordinates

Let us recall the expression for $\tilde{w}_0$ in Cartesian coordinates:

$$\tilde{w}_0(x, y) = -\frac{U_0 h_0}{L^2}(x + i\gamma y) \exp\left(-\frac{x^2 + y^2}{2L^2}\right), \tag{B 1}$$

and hence, in polar coordinates:

$$\tilde{w}_0(\boldsymbol{r} - \boldsymbol{r}_0) = -\frac{U_0 h_0}{L^2} [r\cos\theta - r_0\cos\theta_0 + i\gamma(r\sin\theta - r_0\sin\theta_0)]$$

$$\times \exp\left(-\frac{r^2 + r_0^2 - 2rr_0\cos(\theta - \theta_0)}{2L^2}\right). \tag{B 2}$$

Equation (3.18) consists of a convolution. After inverting $\boldsymbol{r}_0$ and $|\boldsymbol{r} - \boldsymbol{r}_0|$ in it, we find

$$\mathscr{C}_m(r, \theta) = -\frac{U_0 h_0 k_m}{L^2} \exp\left(-\frac{r^2}{2L^2}\right) \int_0^{\infty} r_0 H_0^{(1)}(\mu\beta k_m r_0)$$

$$\times \exp\left(-\frac{r_0^2}{2L^2}\right) \psi(r, r_0, \theta)\, dr_0, \tag{B 3}$$

where

$$\psi(r, r_0, \theta) = \int_0^{2\pi} [r\cos\theta - r_0\cos\theta_0 + i\gamma(r\sin\theta - r_0\sin\theta_0)]$$

$$\times \exp\left(\frac{rr_0\cos(\theta - \theta_0)}{L^2}\right) d\theta_0. \tag{B 4}$$

Performing the variable change $\Theta = \theta - \theta_0$, $d\Theta = -d\theta_0$ and expanding the trigonometric functions yields

$$\psi(r, r_0, \theta) = 2\pi(\cos\theta + i\gamma\sin\theta)\left[r\mathrm{I}_0\left(\frac{rr_0}{L^2}\right) - r_0\mathrm{I}_1\left(\frac{rr_0}{L^2}\right)\right]. \tag{B 5}$$

In the equation above, I_n is the order-n modified Bessel function of the first kind, which for $(n, x) \in (\mathbb{Z}, \mathbb{C})$ can be defined as (cf. Olver *et al.* 2010, § 10.32)

$$I_n(x) = \frac{1}{\pi} \int_0^\pi \cos(n\Theta) e^{x \cos \Theta} \, d\Theta. \tag{B 6}$$

Equation (B 3) hence becomes

$$\mathscr{C}_m = 2\pi k_m \frac{w_0(r, \theta)}{r} \int_0^\infty r_0 H_0^{(1)}(\mu \beta k_m r_0)$$
$$\times \exp\left(-\frac{r_0^2}{2L^2}\right) \left[r I_0 \left(\frac{r r_0}{L^2}\right) - r_0 I_1 \left(\frac{r r_0}{L^2}\right) \right] \, dr_0, \tag{B 7}$$

which yields (6.3).

REFERENCES

ANDREWS, D. G., HOLTON, J. R. & LEOVY, C. B. 1987 *Middle Atmosphere Dynamics*, 1st edn. Academic.

ANDREWS, D. G. & McINTYRE, M. E. 1978 An exact theory of nonlinear waves on a Lagrangian-mean flow. *J. Fluid Mech.* **89** (4), 606–646.

BARREIRO, A. K. & BÜHLER, O. 2008 Longshore current dislocation on barred beaches. *J. Geophys. Res.* **113**, C12004.

BARTON, G. 1989 *Elements of Green's Functions and Propagation: Potentials, Diffusion, and Waves*. Oxford University Press.

BELL, T. H. 1975 Lee waves in stratified flows with simple harmonic time dependence. *J. Fluid Mech.* **67** (4), 705–722.

BRETHERTON, F. P. 1969 On the mean motion induced by internal gravity waves. *J. Fluid Mech.* **36** (4), 785–803.

BÜHLER, O. 2000 On the vorticity transport due to dissipating or breaking waves in shallow-water flow. *J. Fluid Mech.* **407**, 235–263.

BÜHLER, O. 2009 *Waves and Mean Flows*. Cambridge University Press.

BÜHLER, O. 2010 Wave–vortex interactions in fluids and superfluids. *Annu. Rev. Fluid Mech.* **42**, 205–228.

BÜHLER, O. & JACOBSON, T. E. 2001 Wave-driven currents and vortex dynamics on barred beaches. *J. Fluid Mech.* **449**, 313–339.

BÜHLER, O. & McINTYRE, M. E. 1998 On non-dissipative wave-mean interactions in the atmosphere or oceans. *J. Fluid Mech.* **354**, 301–343.

BÜHLER, O. & McINTYRE, M. E. 2003 Remote recoil: a new wave–mean interaction effect. *J. Fluid Mech.* **492**, 207–230.

BÜHLER, O. & MULLER, C. J. 2007 Instability and focusing of internal tides in the deep ocean. *J. Fluid Mech.* **588**, 1–28.

CARTER, G. S., GREGG, M. C. & MERRIFIELD, M. A. 2006 Flow and mixing around a small seamount on Kaena Ridge, Hawaii. *J. Phys. Oceanogr.* **36** (6), 1036–1052.

ECHEVERRI, P. & PEACOCK, T. 2010 Internal tide generation by arbitrary two-dimensional topography. *J. Fluid Mech.* **659**, 247–266.

GARRETT, C. & KUNZE, E. 2007 Internal tide generation in the deep ocean. *Annu. Rev. Fluid Mech.* **39**, 57–87.

HUTHNANCE, J. 1973 Tidal current asymmetries over the Norfolk Sandbanks. *Estuar. Coast. Mar. Sci.* **1** (1), 89–99.

KING, B., ZHANG, H. P. & SWINNEY, H. L. 2009 Tidal flow over three-dimensional topography in a stratified fluid. *Phys. Fluids* **21** (11), 116601.

KUNZE, E. & TOOLE, J. M. 1997 Tidally driven vorticity, diurnal shear, and turbulence atop fieberling seamount. *J. Phys. Oceanogr.* **27** (12), 2663–2693.

LEDWELL, J. R., MONTGOMERY, E. T., POLZIN, K. L., ST. LAURENT, L. C., SCHMITT, R. W. & TOOLE, J. M. 2000 Evidence for enhanced mixing over rough topography in the abyssal ocean. *Nature* **403** (6766), 179–182.

LLEWELLYN SMITH, S. G. & YOUNG, W. R. 2002 Conversion of the barotropic tide. *J. Phys. Oceanogr.* **32** (5), 1554–1566.

LLEWELLYN SMITH, S. G. & YOUNG, W. R. 2003 Tidal conversion at a very steep ridge. *J. Fluid Mech.* **495**, 175–191.

LODER, J. W. 1980 Topographic rectification of tidal currents on the sides of Georges bank. *J. Phys. Oceanogr.* **10** (9), 1399–1416.

MAAS, L. R. M. & ZIMMERMAN, J. T. F. 1989*a* Tide-topography interactions in a stratified shelf sea I. Basic equations for quasi-nonlinear internal tides. *Geophys. Astrophys. Fluid Dyn.* **45** (1–2), 1–35.

MAAS, L. R. M. & ZIMMERMAN, J. T. F. 1989*b* Tide-topography interactions in a stratified shelf sea II. Bottom trapped internal tides and baroclinic residual currents. *Geophys. Astrophys. Fluid Dyn.* **45** (1–2), 37–69.

MCINTYRE, M. E. & NORTON, W. A. 1990 Dissipative wave-mean interactions and the transport of vorticity or potential vorticity. *J. Fluid Mech.* **212**, 403–435.

MULLER, C. J. & BÜHLER, O. 2009 Saturation of the internal tides and induced mixing in the abyssal ocean. *J. Phys. Oceanogr.* **39** (9), 2077–2096.

NIKURASHIN, M. & FERRARI, R. 2010*a* Radiation and dissipation of internal waves generated by geostrophic motions impinging on small-scale topography: application to the southern ocean. *J. Phys. Oceanogr.* **40** (9), 2025–2042.

NIKURASHIN, M. & FERRARI, R. 2010*b* Radiation and dissipation of internal waves generated by geostrophic motions impinging on small-scale topography: theory. *J. Phys. Oceanogr.* **40** (5), 1055–1074.

OLVER, F. W. J., LOZIER, D. W., BOISVERT, R. F. & CLARK, C. W. (Eds) 2010 *NIST Handbook of Mathematical Functions*. Cambridge University Press.

PÉTRÉLIS, F., LLEWELLYN SMITH, S. & YOUNG, W. R. 2006 Tidal conversion at a submarine ridge. *J. Phys. Oceanogr.* **36** (6), 1053–1071.

POLZIN, K. L., TOOLE, J. M., LEDWELL, J. R. & SCHMITT, R. W. 1997 Spatial variability of turbulent mixing in the abyssal ocean. *Science* **276** (5309), 93–96.

ROBINSON, R. M. 1969 The effects of a vertical barrier on internal waves. *Deep Sea Res. Oceanogr. Abstracts* **16** (5), 421–429.

ST LAURENT, L. & GARRETT, C. 2002 The role of internal tides in mixing the deep ocean. *J. Phys. Oceanogr.* **32** (10), 2882–2899.

ZEILON, N. 1912 On tidal boundary-waves and related hydrodynamical problems. *Kungl. Svenska Vetenskapsakademiens Handlingar* **47** (4), 3–45.

ZIMMERMAN, J. T. F. 1978 Topographic generation of residual circulation by oscillatory (tidal) currents. *Geophys. Astrophys. Fluid Dyn.* **11** (1), 35–47.

ZIMMERMAN, J. T. F. 1981 Dynamics, diffusion and geomorphological significance of tidal residual eddies. *Nature* **290** (5807), 549–555.